Circulation Research

ORIGINAL RESEARCH

Glycolysis-Mediated Activation of v-ATPase by Nicotinamide Mononucleotide Ameliorates Lipid-Induced Cardiomyopathy by Repressing the CD36-TLR4 Axis

Shujin Wang,* Yinying Han,* Ruimin Liu,* Mengqian Hou,* Dietbert Neumann, Jun Zhang, Fang Wang, Yumeng Li, Xueya Zhao, Francesco Schianchi, Chao Dai, Lizhong Liu, Miranda Nabben, Jan F.C. Glatz, Xin Wu, Xifeng Lu, Xi Li, Joost J.F.P. Luiken

BACKGROUND: Chronic overconsumption of lipids followed by their excessive accumulation in the heart leads to cardiomyopathy. The cause of lipid-induced cardiomyopathy involves a pivotal role for the proton-pump vacuolar-type H^+-ATPase (v-ATPase), which acidifies endosomes, and for lipid-transporter CD36, which is stored in acidified endosomes. During lipid overexposure, an increased influx of lipids into cardiomyocytes is sensed by v-ATPase, which then disassembles, causing endosomal de-acidification and expulsion of stored CD36 from the endosomes toward the sarcolemma. Once at the sarcolemma, CD36 not only increases lipid uptake but also interacts with inflammatory receptor TLR4 (Toll-like receptor 4), together resulting in lipid-induced insulin resistance, inflammation, fibrosis, and cardiac dysfunction. Strategies inducing v-ATPase reassembly, that is, to achieve CD36 reinternalization, may correct these maladaptive alterations. For this, we used NAD^+ (nicotinamide adenine dinucleotide)-precursor nicotinamide mononucleotide (NMN), inducing v-ATPase reassembly by stimulating glycolytic enzymes to bind to v-ATPase.

METHODS: Rats/mice on cardiomyopathy-inducing high-fat diets were supplemented with NMN and for comparison with a cocktail of lysine/leucine/arginine (mTORC1 [mechanistic target of rapamycin complex 1]-mediated v-ATPase reassembly). We used the following methods: RNA sequencing, mRNA/protein expression analysis, immunofluorescence microscopy, (co)immunoprecipitation/proximity ligation assay (v-ATPase assembly), myocellular uptake of [^{3}H]chloroquine (endosomal pH), and [^{14}C]palmitate, targeted lipidomics, and echocardiography. To confirm the involvement of v-ATPase in the beneficial effects of both supplementations, mTORC1/v-ATPase inhibitors (rapamycin/bafilomycin A1) were administered. Additionally, 2 heart-specific v-ATPase-knockout mouse models (subunits V_1G1/V_0d2) were subjected to these measurements. Mechanisms were confirmed in pharmacologically/genetically manipulated cardiomyocyte models of lipid overload.

RESULTS: NMN successfully preserved endosomal acidification during myocardial lipid overload by maintaining v-ATPase activity and subsequently prevented CD36-mediated lipid accumulation, CD36-TLR4 interaction toward inflammation, fibrosis, cardiac dysfunction, and whole-body insulin resistance. Lipidomics revealed C18:1-enriched diacylglycerols as lipid class prominently increased by high-fat diet and subsequently reversed/preserved by lysine/leucine/arginine/NMN treatment. Studies with mTORC1/v-ATPase inhibitors and heart-specific v-ATPase-knockout mice further confirmed the pivotal roles of v-ATPase in these beneficial actions.

CONCLUSION: NMN preserves heart function during lipid overload by preventing v-ATPase disassembly.

GRAPHIC ABSTRACT: A graphic abstract is available for this article.

Key Words: diabetic cardiomyopathies ■ endosomes ■ fibrosis ■ insulin resistance ■ lipid metabolism ■ toll-like receptor 4

In This Issue, see p 475 | Meet the First Author, see p 476 | Editorial, see p 526

Correspondence to: Shujin Wang, PhD, Institute of Life Sciences, School of Basic Medicine, Chongqing Medical University, Chongqing, China, Email shujin.wang@cqmu.edu.cn, or Xifeng Lu, PhD, Clinical Research Center, The First Affiliated Hospital of Shantou University Medical College, Shantou, China, Email xifenglu@stu.edu.cn, or Xi Li, PhD, Institute of Life Sciences, School of Basic Medicine, Chongqing Medical University, Chongqing, China, Email lixi@shmu.edu.cn
*S. Wang, Y. Han, R. Liu, and M. Hou contributed equally.
Supplemental Material is available at https://www.ahajournals.org/doi/suppl/10.1161/CIRCRESAHA.123.322910.
For Sources of Funding and Disclosures, see page 524.

Circulation Research is available at www.ahajournals.org/journal/res

ORIGINAL RESEARCH

Novelty and Significance

What Is Known?

- Increased translocation of fatty acid-transporter CD36 from its endosomal storage site to the cell surface is one of the earliest events in lipid-induced cardiomyopathy.
- Excess lipids entering cardiomyocytes cause the endosomal proton-pump vacuolar-type H^+-ATPase (v-ATPase) to disassemble in V_0 and V_1 subcomplexes reducing the endosomal luminal acidity and storage capacity for CD36 and triggering CD36 translocation to the sarcolemma, thus leading to further enhancement of lipid uptake.
- Incubation of lipid-overloaded cardiomyocytes in vitro with a specific cocktail of 3 amino acids (Lys/Leu/Arg; lysine/leucine/arginine), apart from activating the anabolic master regulator mTORC1 (mechanistic target of rapamycin complex 1), increases mTORC1-v-ATPase interaction and reactivates the v-ATPase pump.

What New Information Does This Article Contribute?

- NAD^+ (nicotinamide adenine dinucleotide)-precursor nicotinamide mononucleotide is gaining popularity as a nutraceutical to improve numerous health aspects, which may also include preservation/restoration of pump function of the lipid-overloaded heart due to glycolysis-mediated v-ATPase reactivation and subsequent internalization of CD36.
- Diacylglycerols (especially in C18:1-enriched diacylglycerols) are the main harmful lipid mediators of lipid-induced cardiomyopathy, and strategies inducing v-ATPase reassembly correct these maladaptive alterations.
- CD36 translocation to the cell surface not only increases lipid uptake into the heart but also causes a parallel induction of inflammation signaling via binding to the inflammatory receptor TLR4 (Toll-like receptor 4), while both of these maladaptive events can be circumvented by reacidification of the endosomes on either lysine/leucine/arginine or nicotinamide mononucleotide supplementation, therefore keeping CD36 intracellularly.

Lipid overconsumption is part of the Western lifestyle and contributes to obesity and type-2 diabetes. In diabetics, heart failure is the main death cause attributed to the consequences of excessive myocardial lipid accumulation. The associated maladaptive state of the heart is named lipid-induced cardiomyopathy. Lipid-transporter CD36 plays a pivotal role in the cause of this disease because of its translocation from endosomes to the cell surface, causing increased myocardial lipid uptake. Luminal acidification by the proton-pump v-ATPase retains CD36 in endosomes. However, during lipid overload, the increased myocellular lipid influx provokes v-ATPase disassembly, an increase in endosomal pH, and the release of CD36 from intracellular storage. Subsequently, CD36 translocates to the sarcolemma where it not only increases lipid uptake but also induces inflammation via binding to the inflammatory receptor TLR4, together culminating in cardiac dysfunction. Thus, reducing CD36 translocation by promoting the reassembly of v-ATPase could prevent or treat lipid-induced cardiomyopathy. Therefore, we supplemented rodent models of lipid overload with nicotinamide mononucleotide, which we found to prevent v-ATPase disassembly via binding with glycolytic enzymes on activation of glycolysis. For comparison, we also applied another treatment (lysine/leucine/arginine cocktail) to induce v-ATPase assembly via a different mechanism (mTORC1-mediated v-ATPase activation). Both treatments successfully and similarly prevented/reversed lipotoxicity, inflammation, fibrosis, and loss of function in the hearts of rodent models of lipid overload. Hence, nutraceutical v-ATPase reassembly inducing strategies could be tested in the first step for the prevention of cardiac dysfunction in obese/diabetic subjects.

Nonstandard Abbreviations and Acronyms

aRCM	adult rat cardiomyocyte
ATGL	adipose triglyceride lipase
BafA	bafilomycin A
DGAT	diacylglycerol acyltransferase
HFD	high-fat diet
HP	high palmitate
IFM	immunofluorescence microscopy
KLR	lysine/leucine/arginine
LFD	low-fat diet
ND	normal diet
NMN	nicotinamide mononucleotide
PLA	proximity ligation assay
TLR4	Toll-like receptor 4
v-ATPase	vacuolar-type H+-ATPase

A Western lifestyle including lipid overconsumption increases the risk for the development of lipid-induced cardiomyopathy. Initially, the chronically increased lipid supply leads to massive lipid accumulation in the heart.[1] This may elicit a pleiotropy of maladaptive cellular processes (referred to as cardiac lipotoxicity), including insulin resistance, inflammation, and contractile

dysfunction.[2,3] The resulting cardiac maladaptation eventually may lead to heart failure and currently is (one of) the foremost death cause(s) related to type-2 diabetes.[4,5]

At the molecular level, the cascade of events starts with increased cellular fatty acid influx via the cardiac fatty acid-transporter CD36.[6,7] In the healthy heart, CD36 is partly present at the cell surface and partly stored intracellularly within endosomes.[8] These endosomes contain a proton-pump complex, named vacuolar-type H^+-ATPase (v-ATPase), which is responsible for acidification of the lumen of these organelles.[9] v-ATPase is made up of 2 subcomplexes: a V_0 subcomplex, forming a membrane-spanning proton channel, and a V_1 subcomplex, containing a rotor-driven proton pump.[10] Luminal acidification is important for various endosomal functions, such as subcellular storage of CD36. We recently discovered that v-ATPase senses the surplus of fatty acids that enter the cardiomyocytes, on which V_1 disassembles from V_0 to drift away into the cytoplasm. Subsequently, the endosomes lose their acidity and a vesicle budding process is initiated to translocate CD36 to the sarcolemma, leading to progressive myocardial lipid uptake and accumulation.[9]

CD36 not only is a facilitator of fatty acid transport across the sarcolemma but also serves various other functions, including initiation of fatty acid signaling via interaction with TLR4 (Toll-like receptor 4). TLR4 by itself recognizes fatty acids as ligands[11] but needs CD36 as a coreceptor for activation on lipid oversupply.[12,13] TLR4 activation results in the induction of cellular inflammation via a pathway including the adaptor protein MyD88 and stress-related kinases, such as p38-MAPK and P42/44-ERK, leading to stimulation of the key inflammatory transcription factor NFκB and production of cytokines.[14,15] This CD36-mediated inflammatory signaling action may aggravate the maladaptive effect of CD36-mediated myocardial lipid accumulation on the functioning of the lipid-overloaded heart.

Keeping CD36 intracellularly could prove an effective strategy to counteract the onset of maladaptive cardiac morphological and functional changes in the heart on the administration of a high-fat diet (HFD) to rodents.[16,17] Preventing CD36 from translocation to the sarcolemma can be achieved by nutraceutical manipulations aimed to induce the reassembly of v-ATPase. One such manipulation includes a cocktail of 3 amino acids (Lys/Leu/Arg, hereafter lysine/leucine/arginine [KLR]) that activates mTORC1 (mechanistic target of rapamycin complex 1) and its binding to V_1, after which this subcomplex reassembles with V_0, thereby reempowering endosomal acidification during excess lipid supply. Applying this cocktail to cardiomyocytes cultured under high palmitate (HP) conditions reverses contractile dysfunction in vitro.[17] Yet, it has not been studied in detail whether and to what extent KLR can combat lipid-induced cardiac contractile dysfunction in vivo.

In the present study, we aimed to test a novel approach to stimulate acidification of endosomes via supplementation with the nutraceutical NAD^+ (nicotinamide adenine dinucleotide) precursor nicotinamide mononucleotide (NMN). NMN has been used as a supplement in rodents and humans to treat several ailments varying from cognitive problems to senescence.[18,19] NAD^+ is suggested to be important for endosomal/lysosomal acidification because it is a cofactor for the glycolytic enzyme PGK1, which has been found associated with these organelles.[20] Furthermore, NAD^+ was found to stimulate ATP production around the endosomes, which could be efficiently used by v-ATPase.[20] However, in this latter investigation, the mechanism of v-ATPase assembly was not studied. Interestingly, there is another link between v-ATPase and glycolytic enzymes in that when glycolytic fluxes are increased, several of these enzymes (eg, aldolase) will bind to v-ATPase subunits, which induces v-ATPase assembly.[21,22] Combining these observations suggests that NMN addition via NAD^+ may increase glycolytic flux, leading not only to ATP production near endosomes but also to v-ATPase assembly.

In the current study, we investigated whether hearts from rodents, fed with a cardiomyopathy-inducing HFD, benefit from supplementation of NMN and whether its beneficial effects involve v-ATPase reassembly, CD36 internalization, lowering of intracellular lipids, lowering of TLR4-mediated inflammation, and finally leading to restoration of cardiac pumping function. The effects of NMN supplementation on these metabolic, morphological, and functional parameters were compared with those of KLR supplementation to investigate whether 2 different mechanisms of v-ATPase assembly (glycolysis-mediated versus mTORC1-mediated) would lead to the same outcomes. Next, we investigated whether the potential beneficial effects of NMN were dependent on v-ATPase by including 2 v-ATPase knockout mouse models. We also applied cardiac lipidomics to investigate which specific lipid metabolites were most associated with high-fat diet–induced cardiomyopathy and the resolution by the supplementations. Finally, we included palmitate-exposed cardiomyocytes, including HL-1 cardiomyocytes, neonatal mice ventricular myocytes, adult mouse cardiomyocytes, and adult rat cardiomyocytes (aRCMs), to investigate the cellular effects of the supplementations on dynamic metabolic properties, such as endosomal acidification, short-term effects of insulin on metabolic signaling, and substrate uptake under conditions of lipid overload. We conclude that v-ATPase reassembly promises to be an attractive strategy to combat lipid-induced cardiomyopathy.

METHODS

Data Availability

Detailed materials and methods are available in the Supplemental Material. All original data that support the findings of this study, experimental materials, and analytic methods are available from the corresponding author upon reasonable request.

RESULTS

KLR and NMN Supplementations as Strategies to Induce v-ATPase Assembly and Endosomal Acidification in the Lipid-Overloaded Heart

NMN is the focus of the study because it has never been investigated in the context of v-ATPase functioning. Yet, we first aimed to establish in the lipid-overloaded heart the effect of KLR treatment, for which we already have insight into the mechanism of v-ATPase reassembly, including mTORC1 activation.[17] However, in that previous study in which the high-fat diet was provided for 12 weeks with the past 4 weeks of treatment with KLR, the control group on HFD without treatment did not develop cardiac dysfunction so that a possible beneficial effect of KLR on preservation of cardiac function could not be established. In the present study, rats were subjected to 12 weeks of LFD or HFD. This period is sufficient to induce v-ATPase disassembly and loss of endosomal acidification in the HFD group.[17] Then, the diet was continued for 6 weeks with or without KLR supplementation (Figure 1A and 1B). In addition, this KLR supplementation was studied in the absence/presence of rapamycin (mTOR inhibitor) or BafA (v-ATPase inhibitor). First, we confirmed that KLR supplementation on top of HFD elevated the plasma levels of these amino acids, whereas plasma levels of most other amino acids remained unaltered (Figure 1C; Figure S1A through S1C). Furthermore, rapamycin and BafA did not affect plasma levels of lysine, leucine, and arginine of most other amino acids. We also confirmed that KLR supplementation resulted in (rapamycin-sensitive) activation of mTORC1 in the heart and phosphorylation of its direct target p70 S6 kinase (Figure 1D).

We applied immunoprecipitation to investigate the v-ATPase assembly state in rat hearts (Figure 1E). HFD and KLR did not alter protein expression levels of mTOR and v-ATPase subunits. In the LFD condition, V_0 and V_1 were assembled. mTORC1 interacted with V_1 (subunit B2) via LAMTOR but did not bind to V_0 (subunits a2 and d1). The mTORC1-V_0 binding was decreased by HFD and reinstalled by KLR. HFD also decreased V_0-V_1 assembly, as displayed by decreased immunoprecipitation between a2 (or d1) with B2, and this was reversed by KLR (Figure 1E). Additionally, immunofluorescence microscopy (IFM) in combination with the proximity ligation assay (PLA; IFM/PLA) showed that in the LFD condition, the assembled v-ATPase was in a supercomplex with mTORC1, which, in its turn, was bound to the small GTPase RHEB (ras homolog expressed in brain; Figure 1F through 1H). This latter protein provides an anchor to bind mTORC1 to endosomal membrane hotspots.[23] The HFD condition caused decreased colocalization of V_0d1 with V_1B2, V_0d1 with mTORC1, and mTORC1 with RHEB, all of which was reversed by KLR in a rapamycin or BafA-dependent manner (Figure 1F through 1H). These PLA assays indicate that KLR supplementation prevented the lipid-mediated disassembly of the mTORC1-v-ATPase supercomplex and disattachment from endosomal membrane hotspots.

As expected, the induction of v-ATPase disassembly by lipids inhibited endosomal acidification, which was measured in HL-1 cardiomyocytes and aRCMs by cellular accumulation of a radiolabeled form of the (bivalent) weak base chloroquine (^{3}H-CHLQ; Figure 1I and 1J), by staining with the acid-sensitive fluorescent dye LysoSensor-Green DND-189 using flow cytometry (Figure 1K and 1L), and by IFM (Figure S1D). All 3 methods confirmed that culturing the cardiomyocytes in the HP medium induced a decrease in endosomal acidification, which was entirely reversed by KLR in a rapamycin/BafA-sensitive manner. This KLR effect was also entirely blocked by a mTORC1 inhibitor other than rapamycin, being Torin-1 (Figure 1K and 1L).

NMN supplementation, in contrast to KLR, has not been used previously as a v-ATPase reassembling strategy, but we hypothesize that NAD^+ can promote v-ATPase assembly by bridging glycolytic enzymes to V_0 and V_1 (Figure 2A). NMN was supplemented for 18 weeks in mice, which simultaneously received HFD (Figure 2B). HFD led to a decrease in NAD^+/NADH (nicotinamide adenine dinucleotide hydrogen) ratio in the heart, as previously reported in drosophila,[24] and NMN was successful in preventing this (Figure 2C; Figure S2A and S2B). Correspondingly, HFD caused decreases in enzymes involved in NAD^+ synthesis and an increase in NAD^+-degrading enzymes, which were largely prevented by NMN (Figure 2D). NMN supplementation also prevented a fall in NAD^+ in HP-exposed HL-1 cardiomyocytes (Figure S2C). Furthermore, NMN successfully prevented HFD/HP-induced v-ATPase disassembly as measured by immunoprecipitation (Figure 2E) and IFM/PLA (Figure 2F), as well as HP-induced endosomal acidification, as assessed by ^{3}H-CHLQ and LysoSensor-Green, which was sensitive to inhibition by BafA (Figure 2G and 2J; Figure S2D). The preservation of v-ATPase assembly by NMN was associated with the preservation of binding of the glycolytic enzyme aldolase to the V_1 subcomplex, which was otherwise lost in the HFD heart (Figure 2E). Aldolase also binds to V_0, but this binding is not influenced by HFD or NMN and, therefore, likely not of regulatory importance in this respect. The necessity of acceleration of glycolytic enzymes, followed by binding to V_1, for restoration of v-ATPase activity by NMN in lipid-overexposed cardiomyocytes is indicated by the loss of NMN-induced endosomal acidification in the presence of the glycolytic inhibitors 2-deoxyglucose or 3-bromopyruvate (Figure 2H through 2J).

To assess whether any beneficial actions of NMN on cardiac parameters of lipid metabolism, inflammation, and cardiac function (to be investigated in the next

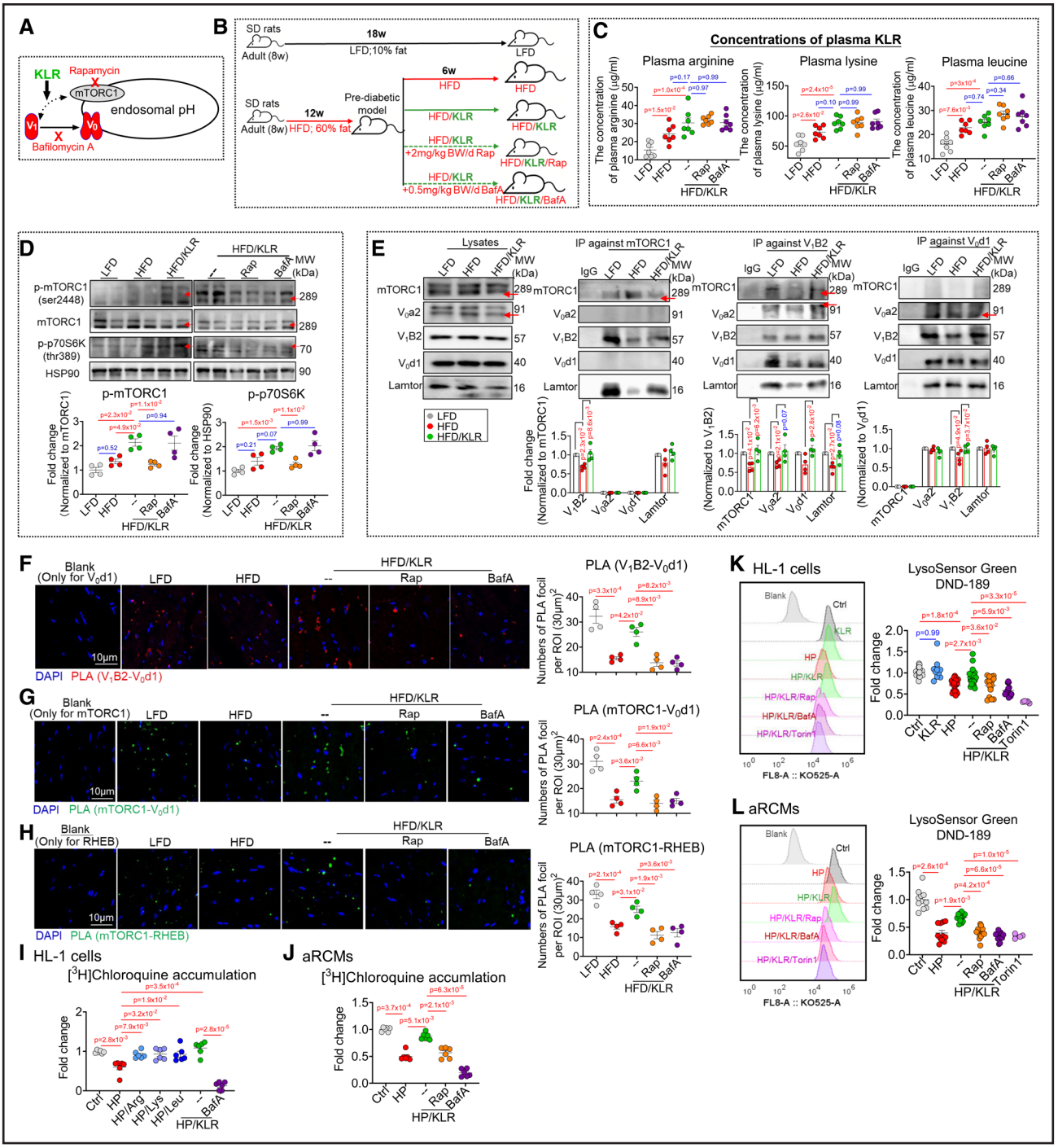

Figure 1. Lysine/leucine/arginine (KLR) supplementation through mTORC1 (mechanistic target of rapamycin complex 1) activation reactivates vacuolar-type H⁺-ATPase (v-ATPase) in the lipid-overloaded heart.

A, Scheme illustrating how KLR supplementation lowers endosomal pH via reactivation of v-ATPase by mTORC1-v-ATPase in a rapamycin/bafilomycin A-sensitive manner. **B**, Experimental design of KLR supplementation: male rats were fed for 18 wk with a low-fat diet (LFD; 10 en% fat), a high-fat diet (HFD; 60 en% fat), HFD with high concentrations of lysine (7 mmol/L), leucine (12 mmol/L), and arginine (10 mmol/L) added to the drinking water during the last 6 wk (HFD/KLR) and with intraperitoneal injection of 2-mg/kg.bw/d rapamycin (HFD/KLR/Rap) or 0.5-mg/kg.bw/d bafilomycin A1 (HFD/KLR/BafA) for the last 6 wk (12 rats in each group). **C**, Plasma concentrations of arginine, leucine, and lysine (n=7). **D**, Activation of mTORC1. Phosphorylation and expression of mTORC1 (p-mTOR ser2448 and total mTORC1) and p70S6K (p-p70S6 kinase Thr389) were detected by Western blotting and quantified (n=4). Representative blots of p-mTORC1 and p-p70S6K are displayed. HSP90: loading control. **E**, Assessment of v-ATPase assembly and complex formation with mTORC1 by immunoprecipitation (IP; n=4). For this, we measured expression levels of mTORC1 and v-ATPase subunits in heart lysates and subsequently performed IPs against mTORC1 and v-ATPase subunits V_1B2 and V_0d1. Representative Western blots and quantification of mTORC1, V_0a2, V_1B2, V_0d1, and LAMTOR1 (late endosomal/lysosomal adaptor 1; subunit of the Ragulator subcomplex and part of the mTORC1 holocomplex) are displayed. **F**, Duolink proximity ligation assay (PLA) staining reveals the assembly status of v-ATPase (V_1B2/V_0d1). **G**, Duolink PLA staining reveals mTORC1-V_0d1 (*Continued*)

Results subsections) were dependent on v-ATPase, we gave NMN as dietary supplement to 2 distinct v-ATPase knockout mouse models: heart-specific full V_0d2 knockout mice (*V0d2*$^{flox/flox}$-*Myhc6*-Cre homozygous strain and V_0d2-mHom; Figure 2K; Figure S3) and heart-specific heterozygous V_1G1 knock-out mice (*V1G1*$^{flox/-}$-*Myhc6*-Cre heterozygous strain and V_1G1-mHet; Figure 2M; Figure S4). Cardiac NAD^+/NADH levels were unaffected by the genotype in HFD-fed mice supplemented with NMN compared with their wild-type littermates (Figure 2L and 2N; Figures S3A, S3B, S4A, and S4B). However, NMN-mediated preservation of v-ATPase assembly and endosomal acidification was impaired in hearts from both v-ATPase knock-out models (Figure 2O through 2T). In conclusion, both KLR and NMN supplementations in vivo rescue and preserve, respectively, the v-ATPase assembly status and optimal endosomal acidification in the lipid-overloaded heart.

v-ATPase Assembly Strategies Downregulate CD36-Mediated Lipid Accumulation and Upregulate Cardiac Insulin Sensitivity

Given that lipid-induced v-ATPase inhibition leads to increased CD36 translocation to the sarcolemma and subsequent myocellular lipid accumulation,[9] we investigated whether v-ATPase reactivation could reverse this process. Using a cell surface biotinylation assay in aRCMs, as well as IFM and immunohistochemistry in rat heart tissue, we observed that HP or HFD induced the translocation of CD36 to the cell surface, which was largely prevented by KLR or NMN supplements in a BafA-sensitive manner (Figure 3A, 3C, and 3E; Figure S5). The involvement of v-ATPase on NMN-mediated CD36 internalization was further confirmed by the loss of this NMN effect in heart tissue from both v-ATPase knockout models (given that the HFD-induced CD36 translocation to the cell surface was not inhibited; Figure 3G and 3I). Furthermore, the beneficial KLR effect was blocked by rapamycin and BafA (Figure 3C). As previously observed,[9,17] HP or HFD did not alter total myocellular CD36 content, nor did any of the treatments (Figure 3A, 3B, 3D, 3F, 3H, and 3J).

CD36 trafficking directly impacts fatty acid uptake rates that were assessed in aRCMs (Figure 3K and 3L). Hence, in line with the CD36 translocation measurements, fatty acid uptake was increased by HP and reversed/preserved by KLR or NMN, whereby the beneficial KLR effects were blocked by both BafA and rapamycin. Alterations in fatty acid uptake have direct consequences for myocellular lipid accumulation. Accordingly, HP exposure in aRCMs caused increased myocellular lipid accumulation, which was reversed/prevented by KLR or NMN in a BafA-sensitive manner (Figure 3M and 3N). Additionally, elevations in myocellular lipid content, as observed in HFD-fed rats/mice, were not seen on KLR or NMN treatment but resurfaced on cotreatment with BafA in rats or v-ATPase knockdown in mice (Figure S6). In conclusion, both in vitro and in vivo experiments showed that KLR and NMN treatments are successful in reversing/preventing HP/HFD-induced CD36 translocation, fatty acid uptake, and lipid accumulation, and these beneficial effects are dependent on v-ATPase reactivation.

The major direct maladaptive effect of myocellular lipid accumulation is insulin resistance.[25] To investigate whether both treatments also had beneficial effects hereon, we investigated in aRCMs the effect of short-term insulin stimulation on (deoxy)glucose uptake, that is, the main hallmark of insulin sensitivity (Figure 3S and 3T). Indeed, the lipid-induced loss of insulin-stimulated glucose uptake was partly reversed/prevented by KLR or NMN, with at least the KLR action being dependent on v-ATPase and mTORC1 activation (ie, inhibitable by rapamycin/BafA).

Diacylglycerol Is the Major Lipid Class Showing Elevated Levels of HFD, and This Maladaptive Change Is Reversed/Prevented by Stimulation of v-ATPase Assembly

To study how v-ATPase activation lowers lipid accumulation and subsequently resolves insulin resistance in lipid-overloaded hearts, we used lipidomics to measure 28 lipid classes and over 620 individual lipid species in each sample. First, partial least-squares discriminant analysis was conducted to give an overview of lipid profiling. This analysis showed clear separations among all conditions (Figure 4A through 4F), indicating that HFD changed the cardiac lipidome signature in rats and mice, and KLR or NMN supplementations caused marked additional changes on top of the HFD, which, in turn, were influenced by pharmacological or genetic v-ATPase reduction.

Figure 1 Continued. interactions in situ. **H**, Duolink PLA staining reveals mTORC1-RHEB (ras homolog expressed in brain) interactions in situ. Image data from **F** through **H** were analyzed for the total number of PLA signals per 30-µm^2 region of interest (ROI). Representative images and their quantification are displayed (n=4; scale bar, 10 µm). **I** through **L**, HL-1 cells and adult rat cardiomyocytes (aRCMs) were cultured for 24 h under following conditions: control (Ctrl in HL-1 cells, no palmitate; Ctrl in aRCMs, 20-µM palmitate complexed to 67-µmol/L bovine serum albumin [BSA], palmitate/BSA ratio 0.3:1), high palmitate (HP in HL-1 cells: 500-µM palmitate complexed to 67-µmol/L BSA, palmitate/BSA ratio 6:1; HP in aRCMs: 200-µM palmitate complexed to 67-µmol/L BSA, palmitate/BSA ratio 3:1), HP supplemented with Lys/Leu/Arg at 1.36/1.84/1.56 mmol/L (HP/KLR), HP/KLR supplemented with 100-nmol/L rapamycin (HP/KLR/Rap), 200-nmol/L torin1 (HP/KLR/Torin1), or 100-nmol/L BafA (HP/KLR/BafA). Directly after the culturing, cells were used for the [^{3}H]chloroquine (CHLQ) accumulation assay (**I** and **J**, n=6) or for staining with LysoSensor-Green DND-189 (**K** and **L**). On LysoSensor staining, cells were examined with flow cytometry analysis (**K**, n=16; **L**, n=8). Data are represented as mean±SEM; exact *P* values were indicated in each figure. IgG indicates immunoglobulin G; and SD, Sprague-Dawley rats.

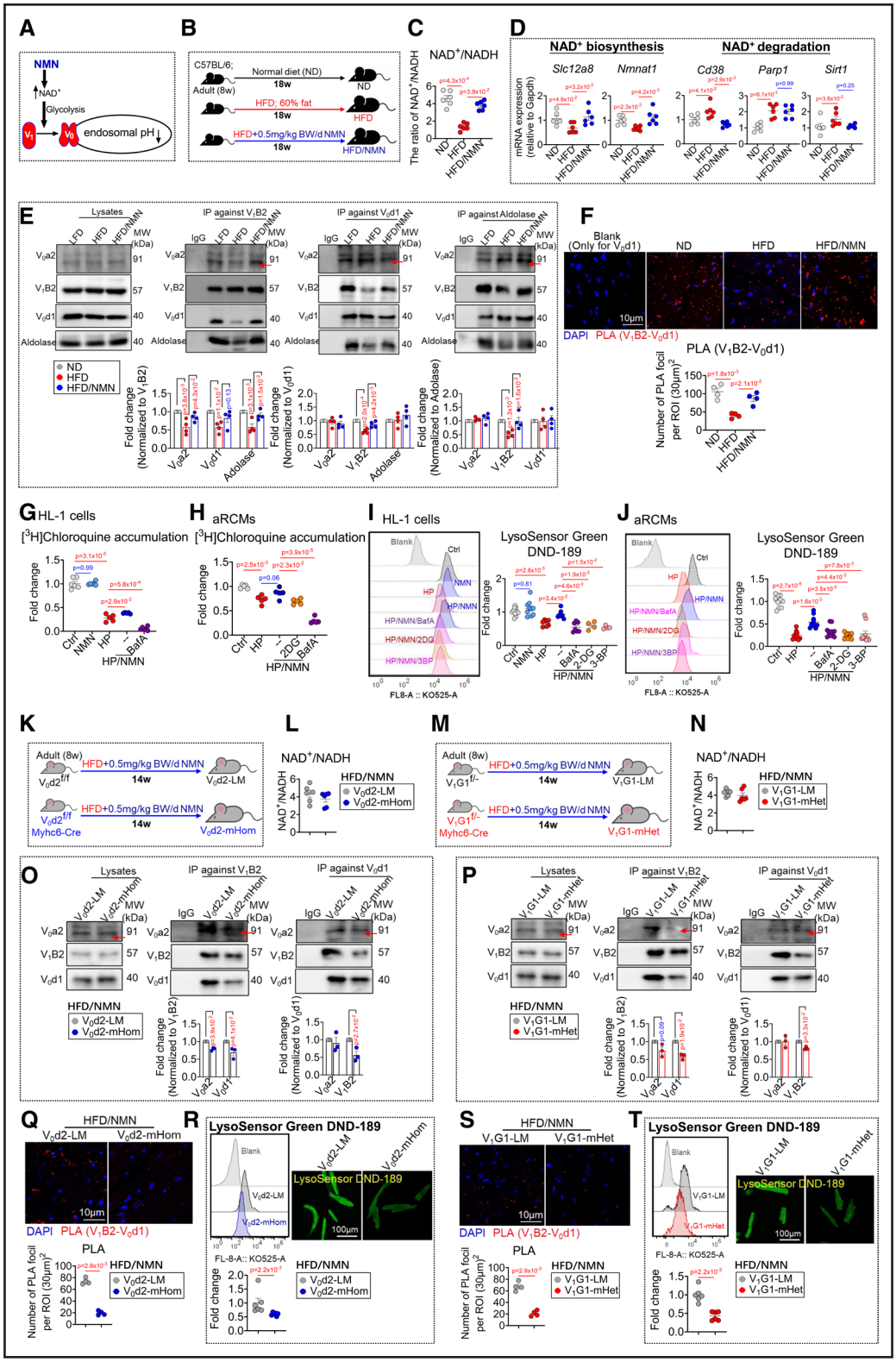

Figure 2. Nicotinamide mononucleotide (NMN) supplementation dependent on conversion to NAD⁺ (nicotinamide adenine dinucleotide) reactivates vacuolar-type H⁺-ATPase (v-ATPase) in the lipid-overloaded heart.

A, Scheme illustrating the effect of NMN on endosomal pH in different experiments. **B**, Workflow of experimental design. Male mice were fed for 18 wk with a normal diet (ND), a high-fat diet (HFD; 60 en% fat), or HFD with drinking water containing 500 mg/L (w/v) of NMN (HFD/NMN; 10 mice in each group). **C**, **L**, and **N**, The ratios of NAD⁺/NADH (nicotinamide adenine dinucleotide hydrogen) in heart tissues of mice (**C**, **L**, and **N**, n=6). **D**, mRNA expression levels of NAD⁺ biosynthesis (*slc12a8* and *nmnat1*) and NAD⁺ degradation genes (*cd38*, *parp1*, and *sirt1*) in heart lysates (n=6). **E**, Assessment of v-ATPase assembly and complex formation with the glycolytic enzyme aldolase by immunoprecipitation (IP; n=4). For this, we measured expression levels of v-ATPase subunits and the glycolytic enzyme aldolase in heart lysates and subsequently (*Continued*)

From all detected lipid classes, we categorized the most abundant ones by log_2-fold changes and calculated the *Z*-score (Figure 4G through 4J). Then, we mainly focused on the lipid classes that showed an increase in HFD in comparison to controls (LFD/ND) because an increase would be the expected direction of change. This criterion excluded (among others) the ceramides, which showed a surprising decrease. Importantly, the most prominent increase impacted by the HFD concerned the diacylglycerols. HFD-induced changes in this lipid class were further analyzed by mass spectrometry (Figure 4K through 4N) and were in line with the lipidomics data. Specifically, these HFD-induced increases in diacylglycerol were reversed/prevented by KLR (Figure 4K) or NMN treatment (Figure 4M). The KLR effect was abolished by rapamycin or BafA (Figure 4L), and the NMN effect was lost in V_1G1-mHet mice (Figure 4N). More detailed analysis of the diacylglycerol class revealed that 2 of the most abundant species were diacylglycerol 18:1-18:1 and diacylglycerol 18:1-18:2, which showed a similar pattern of changes in content as the total diacylglycerol class in response to HFD in combination with KLR or NMN (Figure 4O through 4V). For quantitative analysis of other lipid classes, see Figures S7 and S8.

Having determined that diacylglycerol may be the main mediator of HFD-induced lipotoxicity, and KLR/NMN supplementations successfully decreased diacylglycerol levels in HFD hearts, we aimed to unravel the effects of both supplements on expression levels of all enzymes involved in stepwise diacylglycerol synthesis from fatty acids (Figure 4W; Figure S9). Most of the enzymes in diacylglycerol synthesis and subsequent TAG synthesis/breakdown were upregulated by HFD, with some species-specific differences. Most importantly, KLR or NMN supplementation normalized elevated levels of *Lpin1/2* (phosphatidate phosphatase) isoforms, which mediate the last enzymatic step in diacylglycerol synthesis. Additionally, mRNA/protein levels of DGAT (diacylglycerol acyltransferase) 1/2 and ATGL (adipose triglyceride lipase) were increased by HFD and normalized by KLR/NMN, indicating that both supplementations reversed/prevented maladaptive HFD-induced cycling of fatty acids through the TAG pool (Figure 4X and 4Y; Figure S9). Other normalizing actions of KLR/NMN concerned *Scd1* and *Elovl2/3*, which may help explain the specific changes in the acyl-chain 18:1-enriched diacylglycerol species. For KLR, we investigated whether these actions could be undone by rapamycin or BafA coaddition, and indeed, KLR was ineffective in the presence of either of these compounds (Figure 4X). In conclusion, changes in LPIN and ATGL expression may best explain the HFD-induced increases in myocardial diacylglycerol content and subsequent decreases seen on v-ATPase reactivation by KLR or prevention of v-ATPase deactivation by NMN supplementation.

v-ATPase Assembly Strategies Antagonize Inflammation in the Lipid-Overloaded Heart

In addition to being the major fatty acid transporter in the heart, CD36 also serves as a coreceptor for TLR4. TLR4 by itself does recognize fatty acids as ligands but needs CD36 as a coreceptor in the early events of the inflammatory response when faced with lipid overload.[12] Here, we studied the role of v-ATPase in CD36-mediated TLR4 activation and subsequent inflammatory signaling.

We started these experiments by measuring cell surface localization and myocellular expression of TLR4. The cell surface biotinylation assay using neonatal mice ventricular myocytes, IFM, and immunohistochemistry using heart tissue revealed that HP exposure induced TLR4 translocation to the sarcolemma (Figure 5A, 5C, 5E, 5G, and 5I; Figure S10). This increased TLR4 translocation occurred simultaneously with CD36 translocation, as observed by coimmunostaining of CD36 and TLR4

Figure 2 Continued. performed IPs against v-ATPase subunits (V_1B2 and V_0d1) and aldolase. Representative Western blots and quantification of V_0a2, V_1B2, V_0d1, and aldolase are displayed. **F**, **Q**, and **S**, Duolink proximity ligation assay (PLA) staining reveals the assembly status of v-ATPase (V_1B2/V_0d1). Image data were analyzed for the total number of PLA signals per 30-µm^2 region of interest (ROI). Representative images and their quantification are displayed (**F**, **Q**, and **S**, n=4; scale bar, 10 µm). **G** through **J**, HL-1 cells and adult rat cardiomyocytes (aRCMs) were cultured for 24 h under following conditions: control (Ctrl in HL-1 cells, no palmitate; Ctrl in aRCMs, 20-µM palmitate complexed to 67-µmol/L bovine serum albumin [BSA], palmitate/BSA ratio 0.3:1), high palmitate (HP in HL-1 cells: 500-µM palmitate complexed to 67-µmol/L BSA, palmitate/BSA ratio 6:1; HP in aRCMs: 200-µM palmitate complexed to 67-µmol/L BSA, palmitate/BSA ratio 3:1), HP supplemented with 1-mmol/L NMN (HP/NMN), HP/NMN supplemented with either 1-mM 2-deoxy-D-glucose (HP/NMN/2DG), 10-µM 3-bromopyruvate (HP/NMN/3BP), or 100-nmol/L bafilomycin A (HP/NMN/BafA). Directly after the culturing, cells were used for the [^{3}H]chloroquine (CHLQ) accumulation assay (**G**, n=6; **H**, n=5) or for staining with LysoSensor-Green DND-189 (**I** and **J**). On LysoSensor staining, cells were examined with flow cytometry analysis (**I**, n=12 for Ctrl, NMN, n=8 for HP, HP/NMN, HP/NMN/BafA, and n=4 for HP/NMN/2DG, HP/NMN/3BP; **J**, n=10). **K** through **T**, Experiments in the 2 cardiospecific v-ATPase-knockout (KO) models concerning the effect of NMN supplementation on top of HFD on v-ATPase assembly/activity. **K**, $V_0d2^{flox/flox}$ littermates (V_0d2-LM, n=12) and $V_0d2^{flox/flox}$ Myhc6-Cre knock-out mice (V_0d2-mHom, n=10) were fed with HFD/NMN for 14 wk. **M**, $V_1G1^{flox/-}$ littermates (V_1G1-LM, n=10), and $V_1G1^{flox/-}$ Myhc6-Cre knock-out mice (V_1G1-mHet, n=8) were fed with HFD/NMN for 14 wk. **O** and **P**, Assessment of v-ATPase assembly status in heart lysates from V_0d2-mHom mice (**O**, n=3) and V_1G1-mHet mice (**P**, n=3). For this, we measured expression levels of v-ATPase subunits in heart lysates and subsequently performed IPs against v-ATPase subunits (V_1B2 and V_0d1). Representative Western blots and quantification of V_0a2, V_1B2, and V_0d1 are displayed. **R** and **T**, Assessment of endosomal/lysosomal pH in isolated adult mouse cardiomyocytes (ACMs) from V_0d2-mHom mice (**R**, n=6) and V_1G1-mHet mice (**T**, n=6), respectively. On LysoSensor-Green DND-189 staining, cells were examined with flow cytometry analysis or fluorescence microscopy (scale bar, 100 µm). Data are represented as mean±SEM; exact *P* values were indicated in each figure. DAPI indicates 4′,6-diamidino-2-phenylindole.

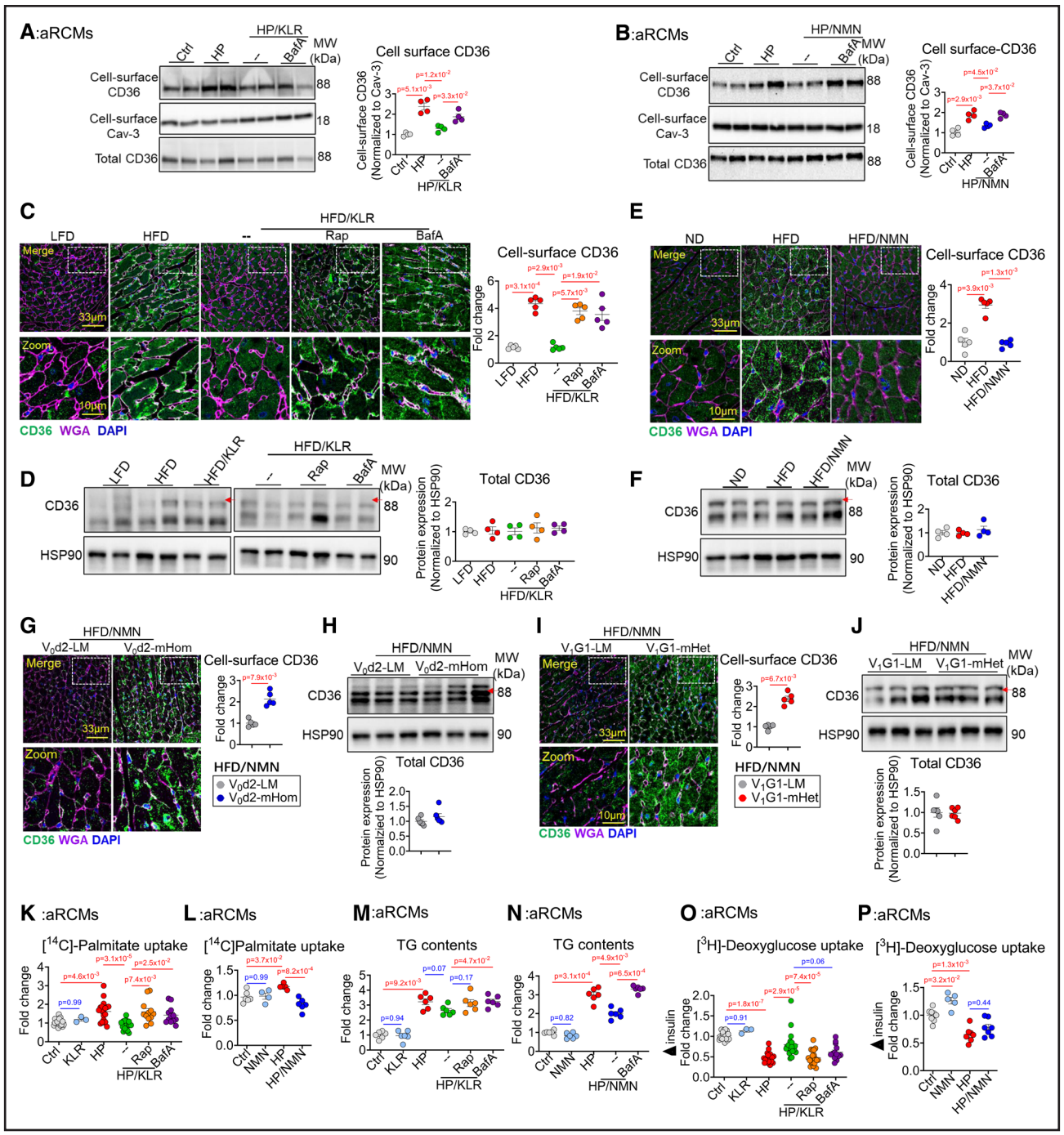

Figure 3. Vacuolar-type H⁺-ATPase (v-ATPase) activation by lysine/leucine/arginine (KLR) and nicotinamide mononucleotide (NMN) supplementation to rats/mice reverses CD36-mediated lipid accumulation in the heart.

A, **B**, and **K** through **P**, In vitro measurement of CD36-mediated lipid accumulation in adult rat cardiomyocytes (aRCMs). aRCMs were cultured for 24 h under the following conditions: control (Ctrl, 20-μM palmitate complexed to 67-μmol/L bovine serum albumin [BSA], palmitate/BSA ratio 0.3:1), high palmitate (HP, 200-μM palmitate complexed to 67-μmol/L BSA, palmitate/BSA ratio 3:1), HP supplemented with Lys/Leu/Arg at 1.36/1.84/1.56 mmol/L (HP/KLR), HP/KLR supplemented with 100-nmol/L rapamycin (HP/KLR/Rap), or 100-nmol/L bafilomycin A (HP/KLR/BafA), HP supplemented with 1-mM NMN (HP/NMN), and HP/NMN supplemented with 100-nmol/L BafA (HP/NMN/BafA). **A** and **B**, Assessment of cell surface CD36 in aRCMs using a biotinylation assay. For this, CD36 was detected by Western blotting in cell surface fractions (cell surface CD36 and caveolin-3) and total lysate (total CD36) and subsequently quantified (**A** and **B**, n=4). **K** and **L**, [14C]palmitate uptake in aRCMs (**K**, n=10; **L**, n=5). **M** and **N**, Assessment of triacylglycerol contents in aRCMs using a commercial kit (**M** and **N**, n=6). **O** and **P**, [3H]Deoxyglucose uptake in aRCMs (**O**, n=10; **P**, n=6). **C** through **J**, In vivo measurement of CD36-mediated lipid accumulation in hearts from experimental groups of rats/mice. The workflows of the animal experiment design are shown in Figures 1 and 2. Experimental groups are (1) rats on 18-wk low-fat diet (LFD; 10 en% fat), rats on 18-wk high-fat diet (HFD; 60 en% fat), rats on HFD with Lys/Leu/Arg supplementation (7/12/10 mmol/L) for last 6 wk (HFD/KLR), and rats on HFD/KLR with rapamycin (HFD/KLR/Rap) or bafilomycin A1 supplementation (HFD/KLR/BafA); (2) wt-mice on 18-wk normal diet (ND), wt-mice on 18-wk HFD (60 en% fat), and wt-mice on HFD with NMN for (*Continued*)

at the cell surface visualized by WGA staining (Figure S11). Furthermore, increased TLR4 translocation was not observed on supplementation with KLR/NMN. When KLR supplementation to HFD-fed rats was accompanied by rapamycin or BafA treatments (Figure 5C; Figure S11A), and when NMN was supplemented to HFD-fed mice from both v-ATPase-knockout (KO) models (Figure 5E, 5G, and 5I; Figure S11B through S11D), these KLR/NMN actions were lost (ie, TLR4 resided at the sarcolemma). TLR4 protein expression in neonatal mice ventricular myocytes or in hearts from rats/mice was not significantly altered by lipid overexposure (HP or HFD) and subsequent KLR/NMN supplementations (Figure 5A, 5B, 5D, 5F, 5H, and 5J). To assess the complex formation of TLR4 with CD36, we performed immunoprecipitation and reversed immunoprecipitation in heart tissue from rats/mice on HFD, as well as PLA/IFM, all of these showing increased CD36-TLR4 association, which was entirely reversed/prevented by KLR or NMN supplementations (Figure 5K through 5P), being agreement with coimmunostaining of CD36 and TLR4 (Figure S11). Confocal microscopy with WGA staining was additionally performed in HP-exposed HL-1 cells supplemented with KLR or NMN, confirming the CD36-TLR4 association also in vitro (Figure S12).

Altogether, these data indicate that lipids induce CD36-TLR4 association at the sarcolemma of cardiomyocytes, and this is reversed by v-ATPase reactivation or prevented by maintenance of v-ATPase activation following KLR or NMN supplementations. v-ATPase reactivation by KLR is additionally dependent on mTORC1.

As mentioned, CD36-TLR4 association is at the start of a proinflammatory response to lipids, which we also investigated further downstream. For this, we measured phosphorylation of the TLR adaptor MYD88 and subsequent activation of proinflammatory signaling pathways involving phosphorylation of p38-MAPK and p42/44-ERK1/2, followed by phosphorylation/activation of the key inflammatory transcription factor NFκB-p65 (Figure 6A through 6D), resulting in the production of inflammatory cytokines (TNF-α, IFN-γ, IL-1β, IL-6, and IL-18; Figure 6E through 6H).

Using Western blotting with phospho-specific antibodies and PCR against cytokines, we observed that HFD increased all these inflammatory-related phosphorylation events in the hearts of rats/mice and the expression of most inflammatory cytokines (Figure 6). There appeared some subtle species-related differences in HFD-induced cytokine production because all cytokines were elevated in rat hearts (Figure 6E), whereas in mouse hearts, TNFα and IL-1β levels were not elevated (Figure 6F). Supplementation of KLR or NMN to these HFD-fed rodents reversed/prevented all these inflammatory effects (Figure 6E and 6F). The KLR action was lost by cotreatment with rapamycin or BafA (Figure 6E), and the NMN action was almost completely lost when HFD was provided to mice from both v-ATPase-KO models (Figure 6F through 6H). The only notable deviation is that in contrast to the V_1G1-mHet mice, the V_0d2-mHom model was ineffective in suppressing the NMN effect on HFD feeding (Figure 6G and 6H). The blocking actions of KLR or NMN supplementation on lipid-induced inflammatory phosphorylation events were largely confirmed in vivo lipid-overloaded hearts (Figure 6A through 6D) and in vitro in HP-exposed HL-1 cardiomyocytes (Figure S13). Moreover, the measurement of plasma levels of inflammatory cytokines yielded similar observations as the myocardial mRNA levels (Figure S14). Finally, by using GSEA and heatmap analysis of RNA sequencing data, we found that the HFD regime induced a full-scale activation of inflammatory pathways in the heart, which was again successfully downregulated by KLR or NMN supplementations (Figure 6I through 6L).

To assess the role of TLR4 in lipid-induced contractile dysfunction of cardiomyocytes, we used the TLR4 inhibitor TAK-242. This inhibitor indeed reduced the phosphorylation of ERK1/2 and NFκB-p65 (Figure 6M) and the production of inflammatory cytokines (Figure 6N). Moreover, mRNA expressions of cardiac hypertrophy markers (eg, *Anp* and *Bnp*; Figure 6O) and dynamic contractile function (ie, sarcomere shortening in Figure 6P) were restored, indicating that inflammation contributes to the overall pleiotropic effects of lipids impacting cardiac function (Figure 6M through 6P).

In conclusion, KLR/NMN supplements successfully prevented/reversed in a v-ATPase reactivation-dependent manner the maladaptive inflammatory actions of HFD in in vitro and in vivo cardiac models.

v-ATPase Assembly Strategies Improve Whole-Body Energy Metabolism and Insulin Sensitivity in HFD-Fed Rodents

To investigate the effect of v-ATPase activating strategies at the level of whole-body metabolism, indirect calorimetry was performed (Figure 7A through 7C). Under both light and dark phases, HFD-fed mice displayed lower CO_2 emission (VCO_2) and respiratory exchange ratio compared with ND-fed mice, and these HFD-induced

Figure 3 Continued. 18 wk (HFD/NMN); (3) $V_0d2^{flox/flox}$ littermates (V_0d2-LM) on HFD/NMN and V_0d2-mHom mice on HFD/NMN; and (5) $V_1G1^{flox/-}$ littermates (V_1G1-LM) on HFD/NMN and V_1G1-mHet mice on HFD/NMN. **C**, **E**, **G**, and **I**, Fluorescence microscopical assessment of CD36 at the cell surface of heart tissue. On display are representative confocal images of hearts stained for CD36 (green), Wheat germ agglutinin (WGA, purple), and nuclei with 4′,6-diamidino-2-phenylindole (DAPI; blue). Scale bar, 33 µm. Cell surface CD36 was quantified by Image-J software (**C**, **E**, **G**, and **I**, n=10 random fields from 5 biologically independent samples per condition). **D**, **F**, **H**, and **J**, Assessment of CD36 protein levels by Western blotting in heart lysates. HSP90: loading control. Representative blots and their quantification are displayed (**D** and **F**, n=4; **H** and **I**, n=6). Data are represented as mean±SEM; exact *P* values were indicated in each figure.

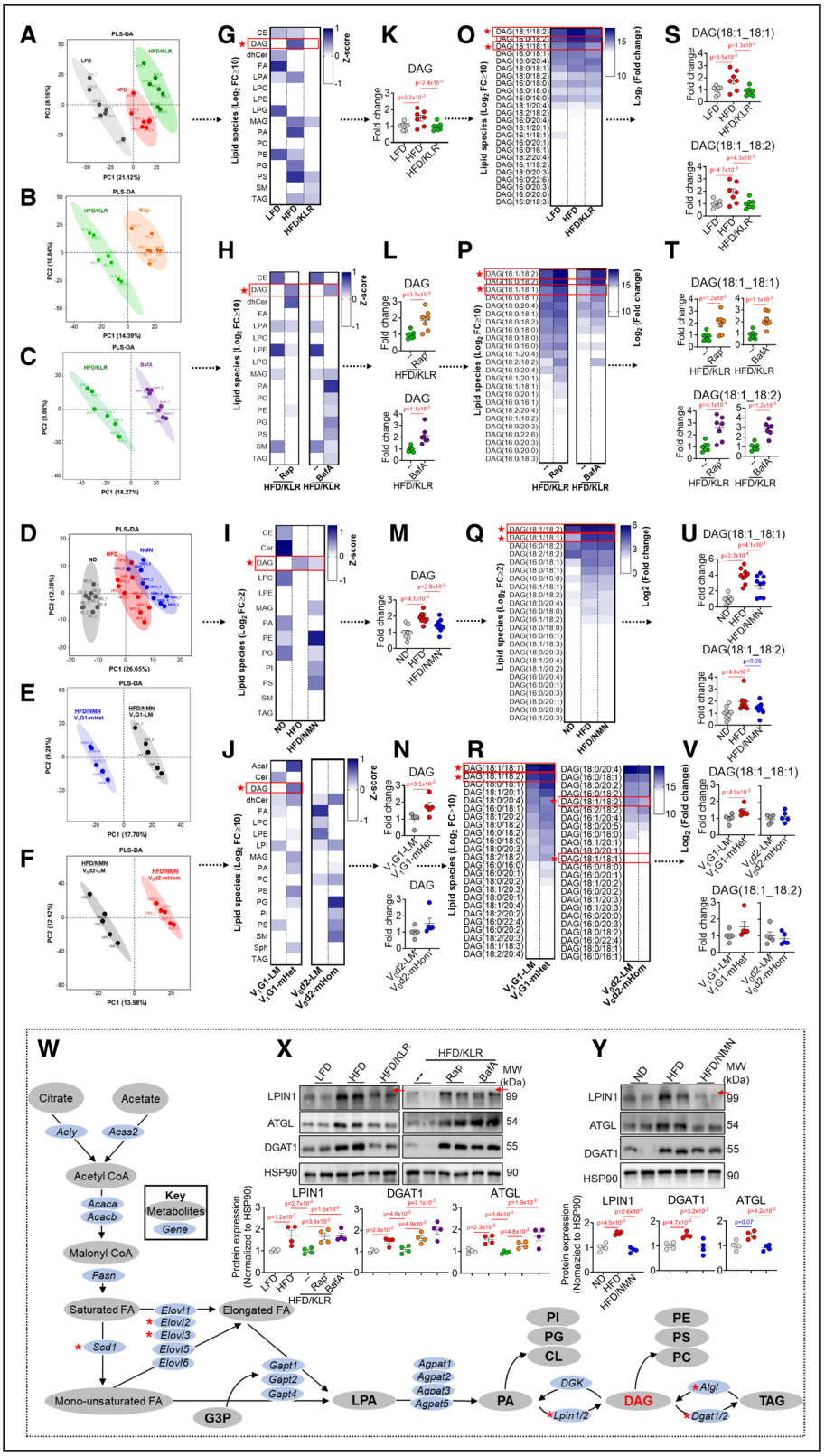

Figure 4. Vacuolar-type H⁺-ATPase (v-ATPase) activation by lysine/leucine/arginine (KLR) and nicotinamide mononucleotide (NMN) supplementation specifically reduces cardiac diacylglycerol (DAG) contents.

A through **F**, Partial least-squares discriminant analysis (PLS-DA) score plots of cardiac lipidomics analysis (**A**–**C**, **G**, and **H**, n=7; **D** and **I**, n=9; and **E**, **F**, and **J**, n=5). **G** through **J**, Lipidomic heatmap showing *Z*-score normalization of main cardiac lipid classes from **A** through **F**. Horizontal rows present different major lipid classes; vertical columns present different experimental animal groups: (1) rats on 18-wk low-fat diet (LFD; 10 en% fat), rats on 18-wk high-fat diet (HFD; 60 en% fat), rats on HFD with Lys/Leu/Arg supplementation (7/12/10 mmol/L) for last 6 wk (HFD/KLR), rats on HFD/KLR with rapamycin (HFD/KLR/Rap), or bafilomycin A1 supplementation (HFD/KLR/BafA); (*Continued*)

changes in VCO_2 and respiratory exchange ratio were largely prevented by NMN supplementation. Notably, this NMN action in HFD-fed mice was almost entirely lost in both V_0d2-mHom mice (Figure 7B) and V_1G1-mHet mice (Figure 7C). In conclusion, we established that the preservation of v-ATPase activation by NMN results in the switching of whole-body energy metabolism in HFD mice back to carbohydrates.

Balanced energy expenditure is often accompanied by the improvement of whole-body insulin sensitivity. In line with the indirect calorimetry data, the glucose tolerance test and systemic insulin sensitivity (insulin tolerance test) of HFD-fed mice were significantly impaired compared with those of controls, and these maladaptive changes were almost entirely reversed/prevented by KLR/NMN supplementation (Figure 7D through 7G). These beneficial KLR actions were partly lost in the presence of rapamycin or BafA (Figure 7D and 7E), and the beneficial NMN action on insulin tolerance test was lost in V_1G1-mHet mice but not in V_0d2-mHom mice (Figure 7H through 7K). Hence, a further conclusion on the beneficial whole-body effects of v-ATPase-reactivating strategies may entail that also KLR and NMN are successful at the level of combating insulin resistance in HFD animals in a v-ATPase-dependent manner. Additionally, the beneficial KLR action depends on the mTORC1-v-ATPase axis. Further beneficial effects of KLR and NMN at the whole-body level, such as body weight, food intake, and weight of organs, are displayed in Figure S15.

v-ATPase Assembly Strategies Ameliorate Lipid-Induced Cardiac Morphological Changes, Fibrosis, and Contractile Dysfunction

To explore whether v-ATPase assembly strategies would ameliorate pathomorphism and cardiac fibrosis in the lipid-overloaded heart, we performed Hematoxylin and Eosin Staining, Periodic Acid-Schiff Staining, Masson Trichrome Staining of cardiac tissue, and qRT-PCR measurement of cardiac hypertrophy/fibrotic biomarkers (Figure 8A and 8H; Figure S16). As expected, the HFD regime caused marked cardiac fibrosis compared with controls (LFD/ND), which was accompanied by a larger heart cross-sectional area (Figure 8A through 8D). Additionally, HFD increased cardiac expression of most fibrosis biomarkers (with subtle species-related differences between rats and mice; Figure 8E and 8H; Figure S16). If the aforementioned beneficial effects of KLR and NMN at the metabolic and inflammatory levels may extend to this morphological level and also to the functional level of the heart, this would indicate that resetting cardiac metabolism via v-ATPase may be a successful strategy to cure heart disease. Indeed, KLR or NMN supplements to rats/mice abolished HFD-induced cardiac structural alterations and fibrosis (Figure 8A and 8D; Figure S16), while the beneficial KLR actions on cardiac pathomorphism and fibrotic gene expression in HFD rodents were lost in the presence of rapamycin or BafA (Figure 8A and 8E). Moreover, these same beneficial actions of NMN were completely lost in V_1G1-mHet mice and largely lost in V_0d2-mHom mice (Figure 8C, 8D, 8G, and 8H; Figure S16).

Contractile dysfunction will inevitably occur as a result of all the abovementioned HFD-induced maladaptive changes. Also, in vitro, that is, in aRCM cultured in HP media, there is marked contractile dysfunction (as earlier established[9,17]), which was counteracted by KLR or NMN supplementation in a manner sensitive to rapamycin (applying to KLR) and to BafA (for both supplements; Figure S17). Consistent with the in vitro findings, compared with controls (LFD/ND), HFD-fed rats/mice developed several cardiac functional and morphological maladaptive changes as established by echocardiography, such as decreased LVEF and LVFS (in rats/mice) and increased LVPWd (in mice) and LVRT (in rats/mice; Figure 8I and 8L; Figure S18). This latter parameter refers to diastolic dysfunction, which is known to be associated with lipid-induced (diabetic) cardiomyopathy.[26] Importantly, KLR or NMN supplementations reversed/prevented these indicators of cardiac dysfunction (Figure 8I and 8J; Figure S18), suggesting that v-ATPase assembly strategies may be of clinical relevance. These beneficial KLR actions were lost in the presence of rapamycin or BafA (Figure 8I; Figure S18), and those of NMN were lost in V_1G1-mHet mice but less in V_0d2-mHom mice (Figure 8K and 8L; Figure S18).

Figure 4 Continued. (2) wt-mice on 18-wk normal diet (ND), wt-mice on 18-wk HFD (60 en% fat), and wt-mice on HFD with NMN for 18 wk (HFD/NMN); (3) $V_1G1^{flox/-}$ littermates (V_1G1-LM) on HFD/NMN and V_1G1-mHet mice on HFD/NMN; and (4) $V_0d2^{flox/flox}$ littermates (V_0d2-LM) on HFD/NMN and V_0d2-mHom mice on HFD/NMN. Relative change of each lipid class is indicated by coloring, and the scale is represented in the color key. **K** through **N**, Assessment of contents of diacylglycerol (DAG) in heart tissues from **G** through **J** (**K** and **L**, n=7; **M**, n=9; and **N**, n=5). Other cardiac lipid classes are displayed in Figures S7 and S8. **O** through **R**, The heatmap of individual DAG species containing MUFA and PUFA acyl tails showing significant changes (log_2-fold changes >10, *Z*-score normalization; **O** and **P**, n=7; **Q**, n=9; and **R**, n=5). **S** through **V**, The contents of the 2 DAG species with the most prominent changes were further assessed in heart tissues from each of the experimental groups (**S** and **T**, n=7; **U**, n=9; and **V**, n=5). **W**, Schematic presentation of the pathway of de novo lipogenesis: genes are represented with blue oval shapes, and metabolites are represented with gray oval shapes. Genes showing significant normalization of expression by KLR or NMN on induction by HFD were denoted with red asterisks. **X** and **Y**, Protein expression of KLR/NMN normalized genes involved in DAG/TAG metabolism in heart tissue. Representative Western blots and quantification of LPIN1 (phosphatidic acid phosphohydrolase1), ATGL (adipose triglyceride lipase), DGAT 1 (diacylglycerol acyltransferase 1), and HSP90 (loading control) are on display (**X** and **Y**, n=4). Cardiac mRNA expressions of these genes and the other indicated lipogenesis-involved genes in **W** are displayed in Figure S9. Data are represented as mean±SEM; exact *P* values were indicated in each figure. MUFA indicates monounsaturated fatty acids; and PUFA, polyunsaturated monounsaturated fatty acids.

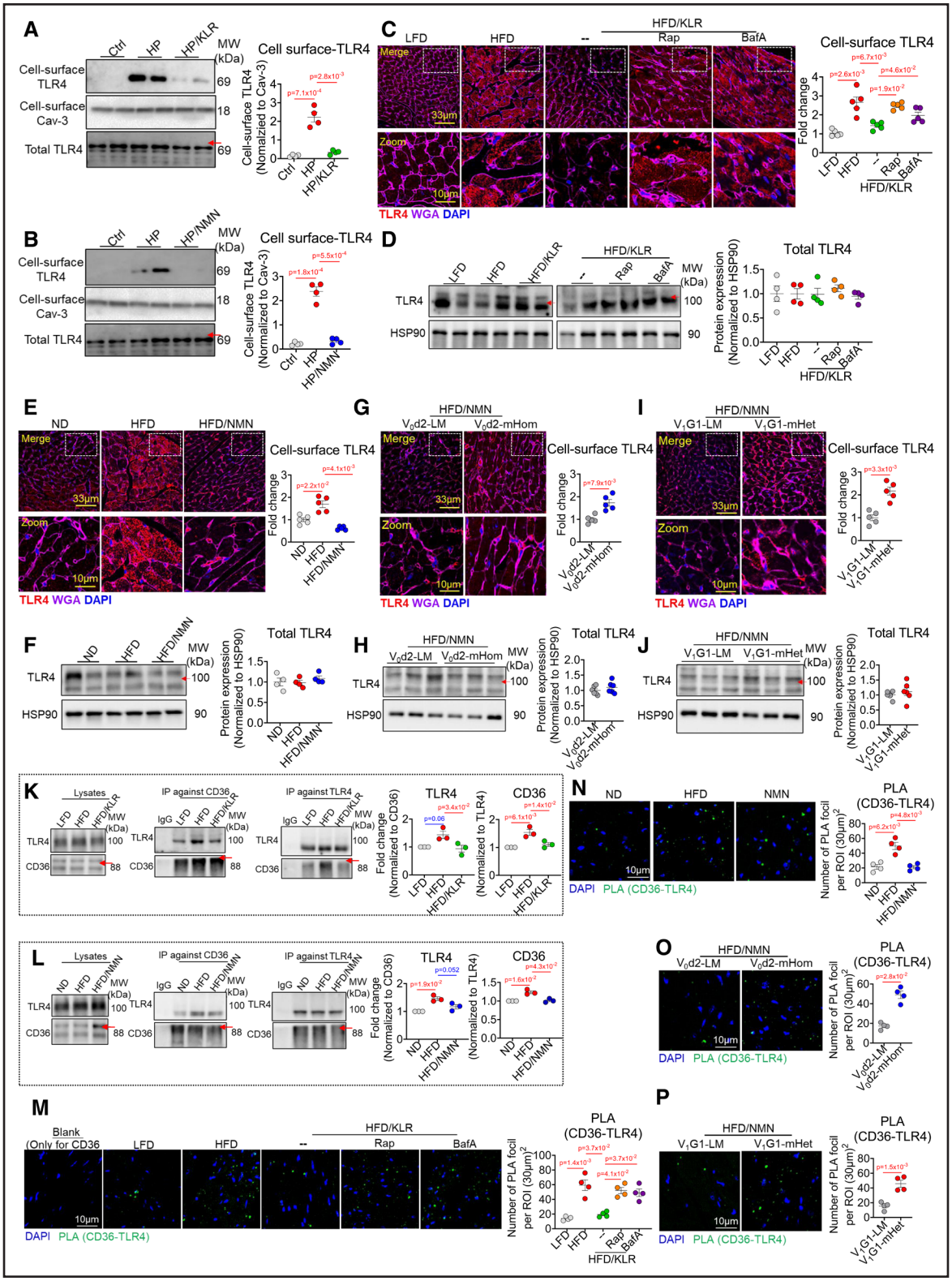

Figure 5. Vacuolar-type H⁺-ATPase (v-ATPase) activation by lysine/leucine/arginine (KLR) and nicotinamide mononucleotide (NMN) supplementation inhibits the interaction of CD36 and TLR4 (Toll-like receptor 4) at the cell surface.

A and **B**, Assessment of cell surface TLR4 in neonatal mice ventricular myocytes (NMVMs) using a biotinylation assay. NMVMs were cultured for 24 h under the following conditions: control (Ctrl), high palmitate (HP), HP/KLR, or HP/NMN. TLR4 was then detected by Western blotting in cell surface fractions (cell surface TLR4 and caveolin-3) and total lysate (total TLR4) and subsequently quantified (**A** and **B**, n=4). **C** through **P**, Assessment of CD36-TLR4 cell surface complex formation in heart tissue. The workflows of animal experiments are shown in Figures 1 and 2. Experimental groups are (1) rats on 18-wk low-fat diet (LFD; 10 en% fat), rats on 18-wk high-fat diet (HFD; 60 en% fat), rats on HFD with Lys/Leu/Arg supplementation (7/12/10 mmol/L) for last 6 wk (HFD/KLR), and rats on HFD/KLR with rapamycin (HFD/KLR/Rap) (*Continued*)

Taken together, consistent with the aforementioned results, these echocardiographic data indicate that the beneficial KLR/NMN actions on cardiac function in lipid-overloaded heart are dependent on proper v-ATPase activity, which, in the case of KLR, is dependent on additional mTORC1 activation.

DISCUSSION

The main aim of the study was to investigate whether therapeutic strategies to induce v-ATPase assembly would be able to improve cardiac contractile dysfunction in rodents on a cardiomyopathy-inducing HFD. For this, we applied the NAD^+-precursor MNM based on our hypothesis that v-ATPase activation could be achieved via acceleration of glycolysis and binding of glycolytic enzymes to specific v-ATPase subunits. Next, we compared the potential beneficial effects of this nutraceutical with dietary supplementation of a KLR cocktail, from which we established that this cocktail induces v-ATPase reassembly via mTORC1 activation. Both strategies reversed/prevented (1) HFD-induced myocellular lipid accumulation (including diacylglycerol synthesis pathway upregulation) and associated insulin resistance, (2) HFD-induced TLR4-CD36 complex formation at the cell surface and subsequent induction of inflammatory pathways leading to myocellular cytokine production, (3) HFD-induced cardiac fibrosis, (4) HFD-induced maladaptive morphological changes and associated loss of contractile function, and (5) both dietary supplements were also successful in preventing/reversing the onset of insulin resistance at the whole-body level in HFD rodents. In the following, the following issues will be discussed in greater detail: (1) evaluation of the in vivo KLR study, (2) mechanisms of the NMN effect, (3) comparison between V_1G1-mHet mice and V_0d2-mHom mice on HFD on their usefulness to evaluate the v-ATPase dependence of the beneficial NMN effects, (4) double role of CD36 in development of lipid-induced cardiac contractile dysfunction, (5) diacylglycerol as harmful lipid mediator, and (6) evaluation whether KLR or NMN supplementation is beneficial not only at the myocardial level but also at the whole-body level.

In Vivo KLR Study

When supplementing KLR to HFD rats, we have used the same concentrations and the same administration route (drinking water) as in our previous in vivo study.[17] However, in that previous study, we applied a shorter HFD regime (12 versus 18 weeks). The 12-week HFD rats displayed myocellular insulin resistance and several maladaptive cardiac morphological changes (ie, increased posterior wall thickness) but not yet loss of cardiac function. Prolonging the HFD to 18 weeks indeed showed decreased cardiac function but also revealed other maladaptive cardiac changes that were previously not studied: increased inflammation and fibrosis. Importantly, KLR supplementation restores v-ATPase assembly/activity and subcellular CD36 retention and subsequently ameliorates cardiac insulin resistance, inflammation, fibrosis, remodeling, and ultimately cardiac dysfunction. The observation that myocellular lipid accumulation and insulin resistance were not reversed by KLR in cardiomyocytes in which v-ATPase-B2 was silenced[17] clearly demonstrates that these beneficial KLR actions are related to v-ATPase reassembly/reactivation. Additionally, mTORC1 activation is necessary, as proven by in vivo treatment with rapamycin, leading to the loss of all beneficial KLR actions. We previously speculated on the mechanism of mTORC1 activation by KLR,[17] in which leucine might act via the leucine-sensor Sestrin-2 and lysine arginine operates through an endosome-centric inside-out mechanism of amino acid sensing.[27] mTORC1 activation by KLR then recruits this kinase complex to the endosomally localized small GTPase RHEB, followed by binding to V_1 and assembly of the v-ATPase holocomplex.[17] In the present study, we demonstrate that KLR not only reverses lipid-induced cardiac morphological changes but also repairs loss of cardiac function, which has far greater clinical significance.

In Vivo NMN Study

NMN was chosen as a novel v-ATPase assembly inducing nutraceutical because it is an efficient NAD^+ precursor. We speculated that the NMN-mediated elevation of the NAD^+/NADH ratio would induce v-ATPase assembly

Figure 5 Continued. or bafilomycin A1 supplementation (HFD/KLR/BafA); (2) wt-mice on 18-wk normal diet (ND), wt-mice on 18-wk HFD (60 en% fat), and wt-mice on HFD with NMN for 18 wk (HFD/NMN); (3) $V_1G1^{flox/-}$ littermates (V_1G1-LM) on HFD/NMN and V_1G1-mHet mice on HFD/NMN; and (4) $V_0d2^{flox/flox}$ LM (V_0d2-LM) on HFD/NMN and V_0d2-mHom mice on HFD/NMN. **C**, **E**, **G**, and **I**, Fluorescence microscopical assessment of TLR4 at the cell surface of heart tissue. On display are representative confocal images of hearts stained for TLR4 (red), Wheat germ agglutinin (WGA, purple), and nuclei with 4′,6-diamidino-2-phenylindole (DAPI; blue). Scale bar, 33 µm. Cell surface TLR4 was quantified with Image-J software (**C**, **E**, **G**, and **I**, n=10 random fields from 5 biologically independent samples per condition). **D**, **F**, **H**, and **J**, Assessment of TLR4 protein levels by Western blotting in heart lysates. HSP90: loading control. Representative blots and quantification are displayed (**D** and **F**, n=4; **H** and **J**, n=6). **K** and **L**, Assessment of complex formation of TLR4 with CD36 by immunoprecipitation (IP). For this, we measured expression levels of both proteins in heart lysates before IP analysis (lysates) and subsequently performed IP against both proteins. Representative Western blots of both proteins in heart lysates and IPs are displayed (**K** and **L**, n=3). **M** through **P**, Duolink proximity ligation assay (PLA) staining reveals CD36-TLR4 interactions in situ. Image data were analyzed for the total number of PLA signals per 30-µm^2 region of interest (ROI). Representative images and their quantification are displayed (**M**–**P**, n=4; scale bar, 10 µm). Data are represented as mean±SEM; exact *P* values were indicated in each figure.

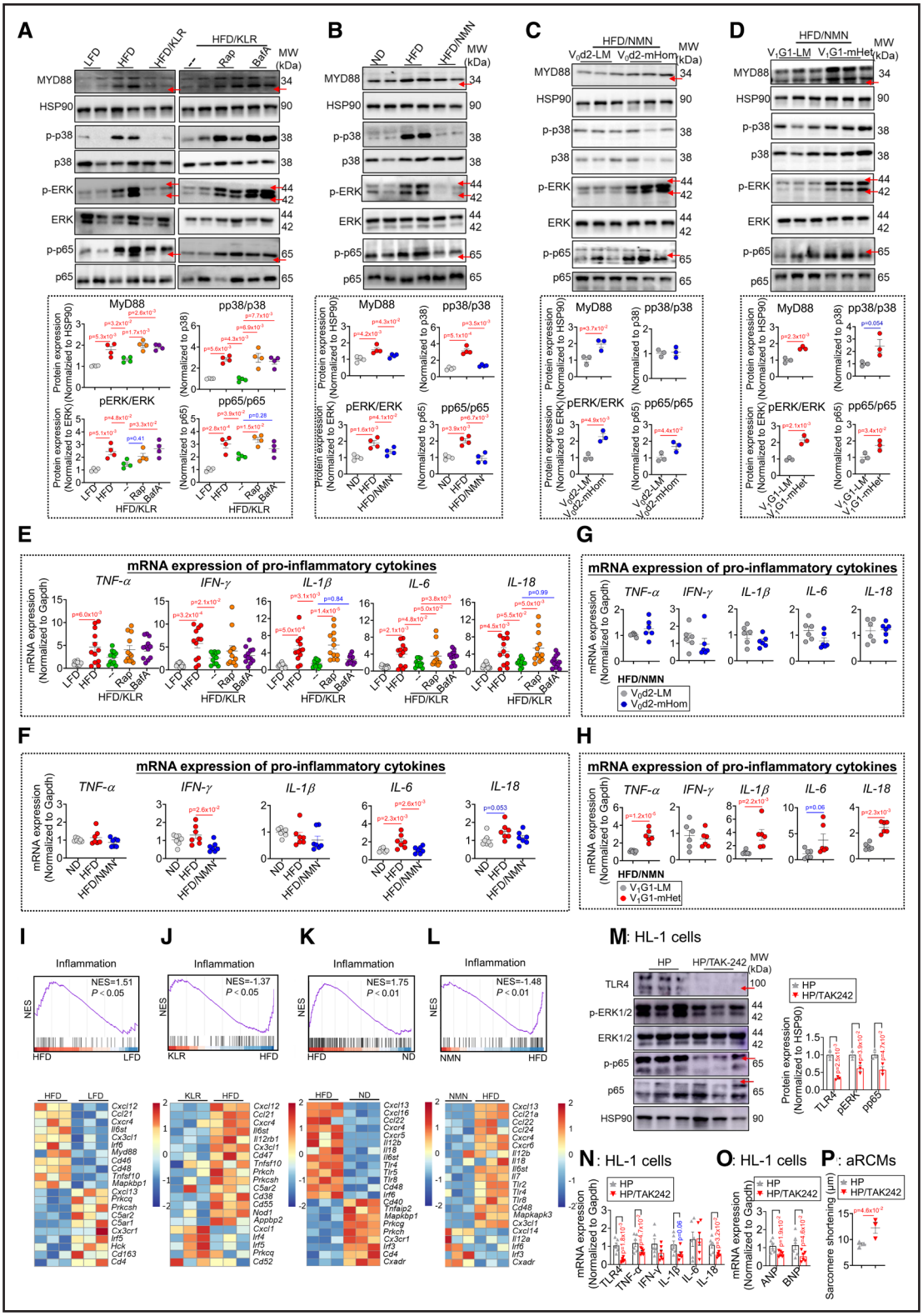

Figure 6. Vacuolar-type H⁺-ATPase (v-ATPase) activation by lysine/leucine/arginine (KLR) and nicotinamide mononucleotide (NMN) supplementation lowers lipid-induced cardiac inflammation.

A through **L**, In vivo inflammatory parameters were assessed in heart tissue from rats/mice. The workflows of the animal experiments are shown in Figures 1 and 2. Experimental groups are (1) rats on 18-wk low-fat diet (LFD; 10 en% fat), rats on 18-wk high-fat diet (HFD; 60 en% fat), rats on HFD with Lys/Leu/Arg supplementation (7/12/10 mmol/L) for last 6 wk (HFD/KLR), and rats on HFD/KLR with rapamycin (HFD/KLR/Rap) or bafilomycin A1 supplementation (HFD/KLR/BafA); (2) wt-mice on 18 wk normal diet (ND), wt-mice on 18-wk HFD (60 en% fat), and wt-mice on HFD with NMN for 18 wk (HFD/NMN); (3) $V_1G1^{flox/-}$ littermates (V_1G1-LM) on HFD/NMN and V_1G1-mHet mice (*Continued*)

via increasing glycolysis based on previous experiments in yeast.[28] In those experiments, glucose was withdrawn and subsequently readded, which reinstalled glycolytic flux followed by binding of glycolytic enzymes to v-ATPase subunits and v-ATPase-reassembly.[21,22] Because glycolytic flux is expected to be low in the lipid-overloaded heart,[29] likely because of low myocellular levels of NAD^+, as observed in drosophila on HFD[24] and confirmed presently (Figure 2), NAD^+ reelevation would be expected to reinstall glycolysis and, thereby, binding of glycolytic enzymes to v-ATPase. This mechanism of NMN action was indeed confirmed to occur, as aldolase was found to bind to the V_1 subcomplex, accompanied by assembly with V_0. Moreover, experiments with glycolytic inhibitors showed that acceleration of glycolysis and glycolytic enzymes proved necessary for NMN-mediated acidification of endosomes in HFD hearts (Figure 2). Subsequently, NMN supplementation successfully blocked all maladaptive lipid-induced actions in the heart (including inflammation, fibrosis, remodeling, and dysfunction), which is similar to the beneficial actions of KLR. NMN supplementation studies in both v-ATPase-KO mouse models showed that all these effects were dependent on v-ATPase, albeit there were some differences between both models, which will be discussed in the next section. Moreover, all beneficial effects of NMN in vitro in HP-cultured cardiomyocytes were lost on cotreatment with BafA. Taken together, NMN supplementation can be applied as a novel v-ATPase reassembling strategy to combat lipid-induced cardiomyopathy.

Difference in Effectiveness of Blocking v-ATPase-Dependent Actions of NMN Between Both Applied Heart-Specific v-ATPase-KO Models

Two v-ATPase-KO models were applied to study the role of v-ATPase in the beneficial effects of NMN in HFD mice. As a control experiment, to confirm whether in the v-ATPase-KO models, the observed losses of NMN effects for the investigated parameters were not due to the presence of Cre recombinase, we reassessed in both v-ATPase-KO models several key parameters by not only comparing the control/HFD+NMN and KO/HFD+NMN experimental groups (as done in Figures 3–8) but also including the flox control/HFD and KO/HFD groups, allowing multiple-comparison statistical analysis. These key parameters included v-ATPase assembly (Figure S19), endosomal pH (Figure S20), CD36-TLR4 association on the cell surface (Figures S21 through S23), inflammatory parameters (Figures S24 and S25), metabolic parameters (Figure S26), or functional contractile parameters (Figures S27 and S28). As it turned out, the observed losses of NMN effects were not attributable to the presence of Cre recombinase in the KO models because no differences were observed between flox control/HFD and KO/HFD for both models (Figures S19 through S28). The comparison between the flox control/HFD and KO/HFD groups also yielded another conclusion: KO of v-ATPase on top of the HFD did not affect any of the studied parameters. This was expected because genetic v-ATPase inhibition and HFD-mediated v-ATPase inhibition would exert the same downstream effects (and, therefore, operate in a nonadditive manner).

However, on MNM administration in combination with HFD, these models were not equally effective in blocking the beneficial NMN actions, with the V_1G1-mHet model being the most consistently effective model. In the V_0d2-mHom model, most beneficial NMN actions in HFD hearts (reversal of lipid accumulation, CD36-mediated TLR4 activation, and inflammation signaling) were effectively impaired, but several other NMN actions (decreases in expression of cytokines/fibrosis markers and improvement of cardiac morphology/function and whole-body insulin resistance) were not blocked. The difference in blocking beneficial NMN effects in both v-ATPase-KO models is first not due to differences in the ability of NMN to preserve v-ATPase assembly and proper acidification in HFD hearts because both aspects were similarly affected in both v-ATPase-KO models.

Figure 6 Continued. on HFD/NMN; and (4) $V_0d2^{flox/flox}$ LM (V_0d2-LM) on HFD/NMN and V_0d2-mHom mice on HFD/NMN. **A** through **D**, Assessment of MyD88-induced inflammatory signaling actions in heart tissues using Western blotting and subsequent quantification (**A** and **B**, n=4; **C** and **D**, n=6). On display are representative blots of MyD88, p-p38, total p38, p-ERK, total ERK, p-NFκB-p65 (p-p65), NF-κB-p65 (p65), and HSP90 (as loading control). **E** through **H**, mRNA expression levels of proinflammatory cytokines, including TNF-α, IFN-γ, IL-1β, IL-6, and IL-18 in heart tissue (**E**, n=10; **F**, n=6; and **G** and **H**, n=7). **I** through **L**, Gene Set Enrichment Analysis (GSEA) of the RNA sequencing (RNA-seq) data from heart tissues were shown in normalized enrichment score (NES), and the heatmap showed expressions of genes associated with inflammation (**I**–**L**, n=3). **M** through **P**, In vitro effects of TLR4 (Toll-like receptor 4) inhibitor on inflammatory signaling actions and contractile function in lipid-overloaded cardiomyocytes. **M** through **O**, HL-1 cells were cultured for 24 h under the following conditions: high palmitate (HP, 500-μM palmitate complexed to 67-μmol/L BSA, palmitate/BSA ratio 6:1) and HP supplemented with 100-nmol/L TAK-242 (the specific TLR4 inhibitor, HP/TAK242). Directly after the culturing, cells were used for assessing TLR4-mediated inflammatory signaling actions in heart tissues using Western blotting (**M**, representative blots and its quantifications of TLR4, p-ERK, total ERK, p-NFκB-p65 [p-p65], NF-κB-p65 [p65], and HSP90 [as loading control]; n=3) and RT-qPCR (**N**, mRNA expression levels of proinflammatory cytokines, including TNF-α, IFN-γ, IL-1β, IL-6, and IL-18; **O**, mRNA expression levels of cardiac fibrotic markers, *ANP* and *BNP*; n=6). **P**, Adult rat cardiomyocytes (aRCMs) were cultured for 24 h under the following conditions: high palmitate (HP, 200-μM palmitate complexed to 67-μmol/L bovine serum albumin [BSA], palmitate/BSA ratio 3:1) and HP supplemented with 100-nmol/L TAK-242 (HP/TAK242). Directly after the culturing, cells were video-imaged during 1-Hz electrostimulation for the assessment of contractile parameters (eg, sarcomere shortening). n=3; imaging of 10 cells per condition. Data are represented as mean±SEM; exact *P* values were indicated in each figure.

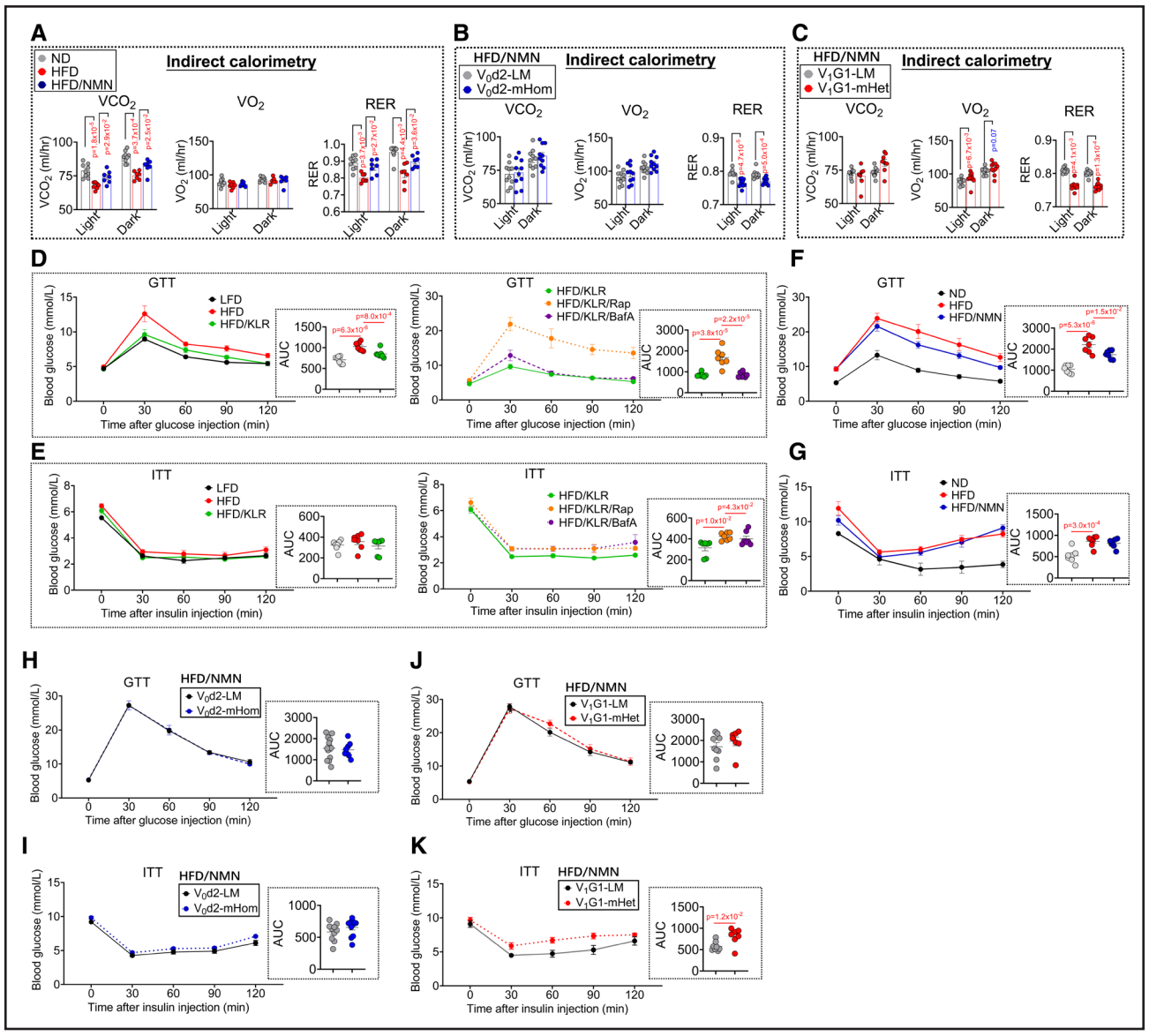

Figure 7. Vacuolar-type H⁺-ATPase (v-ATPase) activation by lysine/leucine/arginine (KLR) and nicotinamide mononucleotide (NMN) supplementation improves energy expenditure and insulin sensitivity.

A through **C**, Assessment of basal indirect calorimetry in mice from different experimental groups during light and dark periods. Experimental animal groups are (1) wt-mice on 18-wk normal diet (ND), wt-mice on 18-wk high-fat diet (HFD; 60 en% fat), and wt-mice on HFD with NMN for 18 wk (HFD/NMN); (2) $V_0d2^{flox/flox}$ littermates (V_0d2-LM) on HFD/NMN and V_0d2-mHom mice on HFD/NMN; and (3) $V_1G1^{flox/-}$ LM (V_1G1-LM) on HFD/NMN and V_1G1-mHet mice on HFD/NMN. The workflows of the animal experiments are shown in Figure 2. For each of the indirect calorimetry parameters (carbon dioxide generation [VCO_2], oxygen consumption [VO_2], and respiratory exchange ratio [RER]), the temporal changes over the day and the 24-h means are on display (**A**, n=8 for ND and n=7 for HFD and HFD/NMN; **B**, n=10; and **C**, n=8). **D** through **K**, Assessment of in vivo insulin sensitivity. Additional experimental animal groups are (**D** and **E**): rats on 18-wk low-fat diet (LFD; 10 en% fat), rats on 18-wk high-fat diet (HFD; 60 en% fat), rats on HFD with Lys/Leu/Arg supplementation (7/12/10 mmol/L) for last 6 wk (HFD/KLR), and rats on HFD/KLR with rapamycin (HFD/KLR/Rap) or bafilomycin A1 supplementation (HFD/KLR/BafA). **D**, **F**, **H**, and **J**, Glucose tolerance test (GTT) and its area under the curve (AUC; **D** and **F**, n=7; **H**, n=12 for V_0d2-LM and n=8 for V_0d2-mHom; and **J**, n=9 for V_1G1-LM and n=7 for V_1G1-mHet). **E**, **G**, **I**, and **K**, Insulin tolerance test (ITT) and its AUC (**D** and **F**, n=7; **H**, n=12 for V_0d2-LM and n=8 for V_0d2-mHom; and **J**, n=9 for V_1G1-LM and n=7 for V_1G1-mHet). Data are represented as mean±SEM; exact *P* values were indicated in each figure.

This might seem surprising because of the use of homozygous KO mice for the d2 subunit and heterozygous KO mice for the G1 subunit. The G1 subunit has expectedly no other isoforms in the heart. In contrast, the rodent heart carries next to the d2 subunit and also the d1 isoform, perhaps in equal abundance (Figure S4).

As to the differences in loss of NMN-mediated beneficial actions between both v-ATPase-KO models, this is still an unresolved question and a limit of the study. Perhaps, NMN could have an impact on other pathways and other cell types that are less affected in the V_0d2-mHom model than in the V_1G1-mHet mice.

ORIGINAL RESEARCH

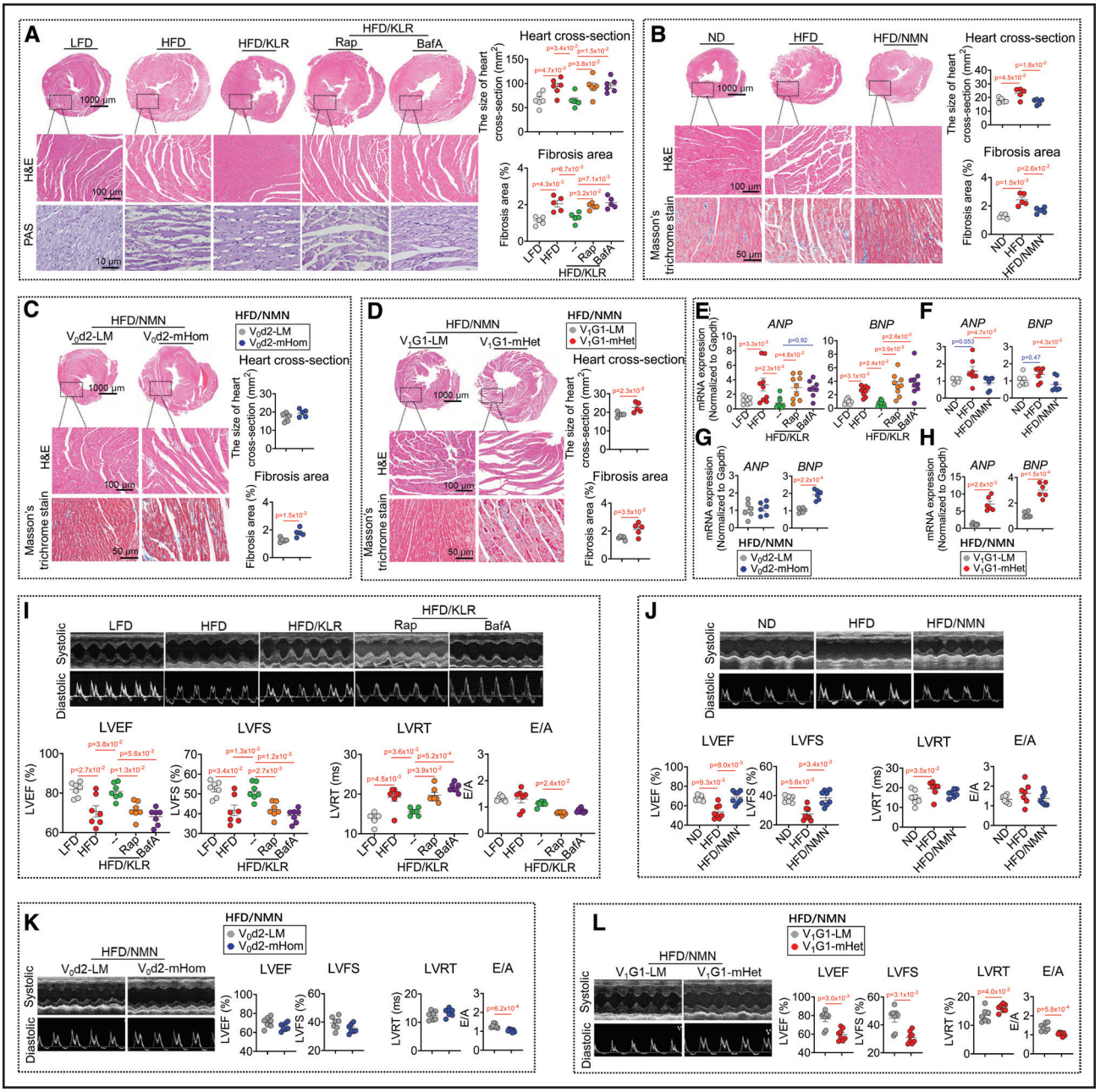

Figure 8. Vacuolar-type H+-ATPase (v-ATPase) activation by lysine/leucine/arginine (KLR) and nicotinamide mononucleotide (NMN) supplementation ameliorates lipid-induced cardiac fibrosis and dysfunction.

A through **D**, Assessment of histopathologic changes in heart tissue from rats/mice from different experimental groups: (1) rats on 18-wk low-fat diet (LFD; 10 en% fat), rats on 18-wk high-fat diet (HFD; 60 en% fat), rats on HFD with Lys/Leu/Arg supplementation (7/12/10 mmol/L) for last 6 wk (HFD/KLR), and rats on HFD/KLR with rapamycin (HFD/KLR/Rap) or bafilomycin A1 supplementation (HFD/KLR/BafA); (2) wt-mice on 18-wk normal diet (ND), wt-mice on 18-wk HFD (60 en% fat), and wt-mice on HFD with NMN for 18 wk (HFD/NMN); (3) $V_0d2^{flox/flox}$ littermates (V_0d2-LM) on HFD/NMN and V_0d2-mHom mice on HFD/NMN; and (4) $V_1G1^{flox/-}$ LM (V_1G1-LM) on HFD/NMN and V_1G1-mHet mice on HFD/NMN. The work flows of the animal experiments are shown in Figures 1 and 2. Histopathologic changes were evaluated by Hematoxylin and Eosin (H&E; scale bar, 100 μm), Periodic Acid-Schiff (PAS; scale bar, 50 μm), and Masson Trichrome staining (scale bar, 50 μm). Quantifications of surface areas from heart cross-sections (H&E staining; **A**, n=6; **B**–**D**, n=5) and fibrosis areas from PAS staining and Masson Trichrome staining (**A**–**D**, n=5). **E** through **H**, Relative mRNA expression levels of cardiac fibrotic markers including ANP (atrial natriuretic peptide) and BNP (brain natriuretic peptide) in heart tissues (**E**, n=9; **F**–**H**, n=6). Other cardiac fibrotic markers are displayed in Figure S16. **I** through **L**, Cardiac function was evaluated by echocardiography. On display are representative images for measurement of systolic parameters: left ventricular ejection fraction (LVEF), left ventricular fractional shortening (LVFS), and measurement of diastolic parameters: ratio between early (E) and late (atrial: A) ventricular filling velocity (E/A ratio) and isovolumic relaxation time (IVRT; **I**, n=7; **J**, n=8 for systolic parameters and n=7 for diastolic parameters; **K**, n=7; and **L**, n=8). Other in vivo echocardiographic parameters are displayed in Figure S18. Data are represented as mean±SEM; exact *P* values were indicated in each figure.

Double Role of CD36 in Development of Lipid-Induced Cardiac Contractile Dysfunction

We have already established earlier that the maladaptively increased fatty acid transport function of CD36 plays a crucial role in the development of contractile function in lipid-overloaded cardiomyocytes both in vitro[30] and in vivo.[31] This transport function is not only increased by the increase in lipid supply itself but also by lipid-induced v-ATPase disassembly and subsequent CD36 translocation[9] and will lead to progressive lipid (diacylglycerol) accumulation and onset of insulin resistance (see next section). Also, another function of CD36, being a coactivator of TLR4, is crucially involved in lipid-induced cardiac contractile dysfunction. CD36 translocation to the cell surface is accompanied by TLR4 translocation, after which both proteins interact to activate MYD88 at the start of inflammatory signaling and production of inflammatory cytokines. Besides the fatty acid transport function, also, this TLR4 coactivator function of CD36 appears to play a crucial role in lipid-induced cardiac contractile dysfunction based on the observation that TAK-242 prevents the production of hypertrophic factors and loss of contractility in HP-treated cardiomyocytes. Hence, it is the combined action of maladaptive lipid accumulation, lipid-induced insulin resistance, and lipid-induced inflammation that sets the heart on a path to contractile dysfunction. In conclusion, the loss of v-ATPase-mediated subcellular CD36 retention acts as a double-edged sword in the onset of lipid-induced cardiac dysfunction. Finally, the power of v-ATPase assembling strategies, such as NMN, lies in the fact that all these CD36-mediated actions are simultaneously blocked.

Diacylglycerol as Harmful Lipid Species Mediating Lipid-Induced Insulin Resistance

Using lipidomics, diacylglycerol was unmasked to be among the main fatty acid metabolites to be elevated by HFD and normalized by KLR or NMN treatment, while this normalization was lost in v-ATPase-KO mice. This is in line with the general view regarding the role of diacylglycerol in the onset of lipid-induced insulin resistance. This view entails that diacylglycerol would activate members of the subfamily of novel PKCs, thereby inducing a signaling cascade leading to inhibitory Ser/Thr phosphorylations of the insulin receptor and subsequent blockade of the canonical insulin signaling pathway.[32,33] In contrast, ceramides, another group of established mediators of lipid-induced insulin resistance/inflammation,[34] were not associated with changes in disease states following HFD and treatments, for reasons that we do not entirely understand. Perhaps, the specific upregulation of Lpins redirects the extra incoming fatty acids in HFD hearts specifically to diacylglycerol synthesis and away from other lipid metabolic pathways. Moreover, TAG breakdown by upregulated ATGL in HFD hearts might contribute to increased diacylglycerol levels.

One would expect that dipalmitoyl diacylglycerols would be the major subclass of diacylglycerol to be upregulated, which would reflect the lipid composition of the HFD (with palmitate as the predominant fatty acid). Instead, diacylglycerol 18:1-18:1 and diacylglycerol 18:1-18:2 were mainly upregulated. This might be a consequence of the specific upregulation of *Scd1* (desaturation) and *Elovl2/3* (elongation). Whether these oleate-enriched diacylglycerols are more potent PKC activators (and insulin resistance inducers) than their palmitate-enriched counterparts is not known. In conclusion, the prominent upregulation of diacylglycerol 18:1-18:1/diacylglycerol 18:1-18:2 in the functionally impaired HFD heart and subsequent downregulation on KLR/NMN treatment associated with restored/preserved cardiac function may suggest that these lipids may be important harmful mediators of lipid overload.

v-ATPase Assembly Strategies to Reverse the Negative Consequences of Lipid Overload Are Not Only Beneficial to the Heart But Also at the Whole-Body Level

CD36 is not only an important fatty acid transporter in the heart but also in skeletal muscle, in which latter tissue it is also stored for a large part intracellularly within endosomes.[35] Hence, similar to the heart, v-ATPase activation would likely serve as a gatekeeper for CD36 also in muscle. The similarity between heart and muscle with respect to CD36 dynamics even extends to the response to lipid overload, that is, when sarcolemmal CD36 translocation is increased.[36] Hence, it is likely that KLR or NMN supplementation improves maladaptive lipid-induced changes not only in the heart but also in muscle. Because skeletal muscle, by virtue of its large contribution to total body mass, is a major regulator of total body (lipid) metabolism, improvement of muscle lipid metabolism by KLR or NMN administration is expected to have beneficial effects at the whole-body level. Accordingly, we show in this study that in HFD animals, there is a switch back to carbohydrate utilization at the whole-body level in combination with an improvement in insulin resistance. Taken together, v-ATPase has a central role in regulating lipid metabolism, with its assembly status being an excellent target to improve maladaptive lipid-induced alterations not only at the level of the heart but also at that of the whole body.

ARTICLE INFORMATION

Received July 16, 2023; revision received January 16, 2024; accepted January 23, 2024.

Affiliations

Institute of Life Sciences, School of Basic Medicine, Chongqing Medical University, China (S.W., Y.H., R.L., M.H., J.Z., X.Z., X. Li). Department of Genetics and Cell Biology, Faculty of Health, Medicine and Life Sciences, Maastricht University, the Netherlands (S.W., F.W., F.S., M.N., J.F.C.G., J.J.F.P.L.). Department of Ultrasound, Beijing Anzhen Hospital, Capital Medical University, China (R.L.). Department of Pathology (D.N.) and Department of Clinical Genetics (M.N., J.F.C.G., J.J.F.P.L.), Maastricht University Medical Center+, the Netherlands. Tianjin Institute of Industrial Biotechnology, Chinese Academy of Sciences, China (Y.L., X.W.). CAS Key Laboratory of Agro-Ecological Processes in Subtropical Region, Institute of Subtropical Agriculture, Chinese Academy of Sciences (CAS), Changsha, China (C.D., X.W.). Department of Physiology, Shenzhen University Medical School, Shenzhen University, China (L.L.). Cardiovascular Research Institute Maastricht School for Cardiovascular Diseases, Maastricht, the Netherlands (M.N.). Clinical Research Center, First Affiliated Hospital of Shantou University Medical College, China (X. Lu). Department of Infectious Disease, The First Affiliated Hospital of Anhui Medical University, Hefei, China (Y.H.).

Acknowledgments

The authors thank the statistical reviewer and Dr Evan Yi-Wen Yu (Department of Epidemiology, Care and Public Health Research Institute (CAPHRI) Care and Public Health Research Institute, Maastricht University, the Netherlands) for their assistance with the statistical analysis.

Author Contributions

S. Wang, X. Lu, X. Li, and J.J.F.P. Luiken conceptualized, designed, and supervised the study. S. Wang, Y. Han, R. Liu, J. Zhang, F. Wang, M. Hou, Y. Li, F. Schianchi, and X. Lu performed experiments and analyzed the data. S. Wang, X. Zhao, L. Liu, and X. Li provided technical support for the bioinformatics analyses. S. Wang, J.J.F.P. Luiken, D. Neumann, M. Nabben, J.F.C. Glatz, X. Li, and X. Wu wrote the article with input from all authors.

Sources of Funding

The work was supported by grants from the National Natural Science Foundation of China (82100919), the Natural Sciences Foundation of Chongqing (2022NSCQ-MSX0643), and the Scientific and Technological Research Program of Chongqing Municipal Education Commission (KJQN202200445 and KJQN202100410) to S. Wang; the National Natural Science Foundation of China (82170881 and 81870605) to X. Lu; the National Key R&D Program of China (2018YFA0800401), the National Natural Science Foundation of China (82070899, 82000744, and 82011530460), the Natural Sciences Foundation of Chongqing (CSTB2022NSCQ-MSX0827), and the Chongqing Medical University (CQMU) Program for Youth Innovation in Future Medicine (W0046) X. Li; the Dutch Heart Foundation (Dekker grant 2019T041) to M. Nabben; and the Netherlands Organization for Scientific Research (NWO-ALW grant ALWOP.367) to J.J.F.P. Luiken.

Disclosures

None.

Supplemental Material

Major Resources Table
Expanded Materials & Methods
Figures S1–S28
Tables S1–S5
Uncut Gel Blots
References 37–40

REFERENCES

1. Costantino S, Akhmedov A, Melina G, Mohammed SA, Othman A, Ambrosini S, Wijnen WJ, Sada L, Ciavarella GM, Liberale L, et al. Obesity-induced activation of JunD promotes myocardial lipid accumulation and metabolic cardiomyopathy. *Eur Heart J*. 2019;40:997–1008. doi: 10.1093/eurheartj/ehy903
2. Jia G, Hill MA, Sowers JR. Diabetic cardiomyopathy: an update of mechanisms contributing to this clinical entity. *Circ Res*. 2018;122:624–638. doi: 10.1161/CIRCRESAHA.117.311586
3. Tuleta I, Frangogiannis NG. Fibrosis of the diabetic heart: clinical significance, molecular mechanisms, and therapeutic opportunities. *Adv Drug Deliv Rev*. 2021;176:113904. doi: 10.1016/j.addr.2021.113904
4. Joseph JJ, Deedwania P, Acharya T, Aguilar D, Bhatt DL, Chyun DA, Di Palo KE, Golden SH, Sperling LS; American Heart Association Diabetes Committee of the Council on Lifestyle and Cardiometabolic Health; Council on Arteriosclerosis, Thrombosis and Vascular Biology; Council on Clinical Cardiology; and Council on Hypertension. Comprehensive management of cardiovascular risk factors for adults with type 2 diabetes: a scientific statement from the American Heart Association. *Circulation*. 2022;145:e722–e759. doi: 10.1161/CIR.0000000000001040
5. Jia G, DeMarco VG, Sowers JR. Insulin resistance and hyperinsulinaemia in diabetic cardiomyopathy. *Nat Rev Endocrinol*. 2016;12:144–153. doi: 10.1038/nrendo.2015.216
6. Shu H, Peng Y, Hang W, Nie J, Zhou N, Wang DW. The role of CD36 in cardiovascular disease. *Cardiovasc Res*. 2022;118:115–129. doi: 10.1093/cvr/cvaa319
7. Glatz JF, Nabben M, Heather LC, Bonen A, Luiken JJ. Regulation of the subcellular trafficking of CD36, a major determinant of cardiac fatty acid utilization. *Biochim Biophys Acta*. 2016;1861:1461–1471. doi: 10.1016/j.bbalip.2016.04.008
8. Glatz JF, Luiken JJ, Bonen A. Membrane fatty acid transporters as regulators of lipid metabolism: implications for metabolic disease. *Physiol Rev*. 2010;90:367–417. doi: 10.1152/physrev.00003.2009
9. Liu Y, Steinbusch LKM, Nabben M, Kapsokalyvas D, van Zandvoort M, Schonleitner P, Antoons G, Simons PJ, Coumans WA, Geomini A, et al. Palmitate-induced vacuolar-type H^+-ATPase inhibition feeds forward into insulin resistance and contractile dysfunction. *Diabetes*. 2017;66:1521–1534. doi: 10.2337/db16-0727
10. Abbas YM, Wu D, Bueler SA, Robinson CV, Rubinstein JL. Structure of v-ATPase from the mammalian brain. *Science*. 2020;367:1240–1246. doi: 10.1126/science.aaz2924
11. Lancaster GI, Langley KG, Berglund NA, Kammoun HL, Reibe S, Estevez E, Weir J, Mellett NA, Pernes G, Conway JR, et al. Evidence that TLR4 is not a receptor for saturated fatty acids but mediates lipid-induced inflammation by reprogramming macrophage metabolism. *Cell Metab*. 2018;27:1096–1110.e5. doi: 10.1016/j.cmet.2018.03.014
12. Stewart CR, Stuart LM, Wilkinson K, Van Gils JM, Deng J, Halle A, Rayner KJ, Boyer L, Zhong R, Frazier WA, et al. CD36 ligands promote sterile inflammation through assembly of a Toll-like receptor 4 and 6 heterodimer. *Nat Immunol*. 2010;11:155–161. doi: 10.1038/ni.1836
13. Wang Y, Luo W, Han J, Khan ZA, Fang Q, Jin Y, Chen X, Zhang Y, Wang M, Qian J, et al. MD2 activation by direct AGE interaction drives inflammatory diabetic cardiomyopathy. *Nat Commun*. 2020;11:2148. doi: 10.1038/s41467-020-15978-3
14. Lu H, Xu X, Fu D, Gu Y, Fan R, Yi H, He X, Wang C, Ouyang B, Zhao P, et al. Butyrate-producing Eubacterium rectale suppresses lymphomagenesis by alleviating the TNF-induced TLR4/MyD88/NF-κB axis. *Cell Host Microbe*. 2022;30:1139–1150.e7. doi: 10.1016/j.chom.2022.07.003
15. Wang S, Fu W, Zhao X, Chang X, Liu H, Zhou L, Li J, Cheng R, Wu X, Li X, et al. Zearalenone disturbs the reproductive-immune axis in pigs: the role of gut microbial metabolites. *Microbiome*. 2022;10:1–24. doi: 10.1186/s40168-022-01397-7
16. Wang S, Wong LY, Neumann D, Liu Y, Sun A, Antoons G, Strzelecka A, Glatz JF, Nabben M, Luiken JJ. Augmenting vacuolar H^+-ATPase function prevents cardiomyocytes from lipid-overload induced dysfunction. *Int J Mol Sci*. 2020;21:1520. doi: 10.3390/ijms21041520
17. Wang S, Schianchi F, Neumann D, Wong LY, Sun A, van Nieuwenhoven FA, Zeegers MP, Strzelecka A, Col U, Glatz JF, et al. Specific amino acid supplementation rescues the heart from lipid overload-induced insulin resistance and contractile dysfunction by targeting the endosomal mTOR–v-ATPase axis. *Molecular Metabolism*. 2021;53:101293. doi: 10.1016/j.molmet.2021.101293
18. Mills KF, Yoshida S, Stein LR, Grozio A, Kubota S, Sasaki Y, Redpath P, Migaud ME, Apte RS, Uchida K, et al. Long-term administration of nicotinamide mononucleotide mitigates age-associated physiological decline in mice. *Cell Metab*. 2016;24:795–806. doi: 10.1016/j.cmet.2016.09.013
19. Nadeeshani H, Li J, Ying T, Zhang B, Lu J. Nicotinamide mononucleotide (NMN) as an anti-aging health product–promises and safety concerns. *J Adv Res*. 2022;37:267–278. doi: 10.1016/j.jare.2021.08.003
20. Yagi M, Toshima T, Amamoto R, Do Y, Hirai H, Setoyama D, Kang D, Uchiumi T. Mitochondrial translation deficiency impairs NAD^+-mediated lysosomal acidification. *EMBO J*. 2021;40:e105268. doi: 10.15252/embj.2020105268
21. Li M, Zhang CS, Feng JW, Wei X, Zhang C, Xie C, Wu Y, Hawley SA, Atrih A, Lamont DJ, et al. Aldolase is a sensor for both low and high glucose, linking to AMPK and mTORC1. *Cell Res*. 2021;31:478–481. doi: 10.1038/s41422-020-00456-8
22. Lu M, Ammar D, Ives H, Albrecht F, Gluck SL. Physical interaction between aldolase and vacuolar H+-ATPase is essential for the assembly and

activity of the proton pump. *J Biol Chem*. 2007;282:24495–24503. doi: 10.1074/jbc.M702598200
23. Yang H, Jiang X, Li B, Yang HJ, Miller M, Yang A, Dhar A, Pavletich NPJN. Mechanisms of mTORC1 activation by RHEB and inhibition by PRAS40. *Nature*. 2017;552:368–373. doi: 10.1038/nature25023
24. Wen DT, Zheng L, Lu K, Hou WQ. Activation of cardiac Nmnat/NAD+/SIR2 pathways mediates endurance exercise resistance to lipotoxic cardiomyopathy in aging Drosophila. *J Exp Biol*. 2021;224:jeb242425. doi: 10.1242/jeb.242425
25. Boström P, Andersson L, Rutberg M, Perman J, Lidberg U, Johansson BR, Fernandez-Rodriguez J, Ericson J, Nilsson T, Borén J, et al. SNARE proteins mediate fusion between cytosolic lipid droplets and are implicated in insulin sensitivity. *Nat Cell Biol*. 2007;9:1286–1293. doi: 10.1038/ncb1648
26. Urlic H, Kumric M, Vrdoljak J, Martinovic D, Dujic G, Vilovic M, Ticinovic Kurir T, Bozic J. Role of echocardiography in diabetic cardiomyopathy: from mechanisms to clinical practice. *J Cardiovasc Dev Dis*. 2023;10:46. doi: 10.3390/jcdd10020046
27. Zoncu R, Bar-Peled L, Efeyan A, Wang S, Sancak Y, Sabatini DM. mTORC1 senses lysosomal amino acids through an inside-out mechanism that requires the vacuolar H(+)-ATPase. *Science*. 2011;334:678–683. doi: 10.1126/science.1207056
28. Chan CY, Dominguez D, Parra KJ. Regulation of vacuolar H+-ATPase (v-ATPase) reassembly by glycolysis flow in 6-phosphofructo-1-kinase (PFK-1)-deficient yeast cells. *J Biol Chem*. 2016;291:15820–15829. doi: 10.1074/jbc.M116.717488
29. Wright JJ, Kim J, Buchanan J, Boudina S, Sena S, Bakirtzi K, Ilkun O, Theobald HA, Cooksey RC, Kandror KV, et al. Mechanisms for increased myocardial fatty acid utilization following short-term high-fat feeding. *Cardiovasc Res*. 2009;82:351–360. doi: 10.1093/cvr/cvp017
30. Angin Y, Steinbusch LK, Simons PJ, Greulich S, Hoebers NT, Douma K, van Zandvoort MA, Coumans WA, Wijnen W, Diamant M, et al. CD36 inhibition prevents lipid accumulation and contractile dysfunction in rat cardiomyocytes. *Biochem J*. 2012;448:43–53. doi: 10.1042/BJ20120060
31. Ouwens D, Diamant M, Fodor M, Habets D, Pelsers M, El Hasnaoui M, Dang Z, Van den Brom C, Vlasblom R, Rietdijk A. Cardiac contractile dysfunction in insulin-resistant rats fed a high-fat diet is associated with elevated CD36-mediated fatty acid uptake and esterification. *Diabetologia*. 2007;50:1938–1948. doi: 10.1007/s00125-007-0735-8
32. Samuel VT, Petersen KF, Shulman GI. Lipid-induced insulin resistance: unravelling the mechanism. *Lancet*. 2010;375:2267–2277. doi: 10.1016/S0140-6736(10)60408-4
33. Dohm GL. Mechanisms of muscle insulin resistance in obese individuals. *Int J Sport Nutr Exerc Metab*. 2001;11:S64–S70. doi: 10.1123/ijsnem.11.s1.s64
34. Chaurasia B, Summers SA. Ceramides in metabolism: key lipotoxic players. *Annu Rev Physiol*. 2021;83:303–330. doi: 10.1146/annurev-physiol-031620-093815
35. Bonen A, Luiken JJ, Arumugam Y, Glatz JF, Tandon NN. Acute regulation of fatty acid uptake involves the cellular redistribution of fatty acid translocase. *J Biol Chem*. 2000;275:14501–14508. doi: 10.1074/jbc.275.19.14501
36. Luiken JJ, Arumugam Y, Dyck DJ, Bell RC, Pelsers MM, Turcotte LP, Tandon NN, Glatz JF, Bonen A. Increased rates of fatty acid uptake and plasmalemmal fatty acid transporters in obese Zucker rats. *J Biol Chem*. 2001;276:40567–40573. doi: 10.1074/jbc.M100052200
37. Readnower RD, Brainard RE, Hill BG, Jones SP. Standardized bioenergetic profiling of adult mouse cardiomyocytes. *Physiol Genomics*. 2012;44:1208–1213. doi: 10.1152/physiolgenomics.00129.2012
38. Sreejit P, Kumar S, Verma RS. An improved protocol for primary culture of cardiomyocyte from neonatal mice. *In Vitro Cell Dev Biol Anim*. 2008;44:45–50. doi: 10.1007/s11626-007-9079-4
39. Müller TD, Klingenspor M, Tschöp MH. Revisiting energy expenditure: how to correct mouse metabolic rate for body mass. *Nat Metab*. 2021;3:1134–1136. doi: 10.1038/s42255-021-00451-2
40. Mina AI, LeClair RA, LeClair KB, Cohen DE, Lantier L, Banks AS. CalR: a web-based analysis tool for indirect calorimetry experiments. *Cell Metab*. 2018;28:656–666.e1. doi: 10.1016/j.cmet.2018.06.019